

1 **Understanding aerosol composition in a tropical inter-Andean valley** 2 **impacted by agro-industrial and urban emissions**

3

4 Lady Mateus-Fontecha¹, Angela Vargas-Burbano¹, Rodrigo Jimenez*¹, Nestor Y. Rojas¹, German Rueda-
5 Saa², Dominik van Pinxteren³, Manuela van Pinxteren³, Kanneh Wadinga Fomba³, Hartmut Herrmann³

6

7 ¹ Universidad Nacional de Colombia – Bogota, Department of Chemical and Environmental Engineering, Air Quality Research
8 Group, Bogota, DC 111321, Colombia

9 ² Universidad Nacional de Colombia – Palmira, Department of Engineering and Management, Environmental Prospective,
10 Research Group, Palmira, Valle del Cauca 763533, Colombia

11 ³ Leibniz Institute for Tropospheric Research (TROPOS), Atmospheric Chemistry Department (ACD), Permoserstrasse. 15,
12 04318, Leipzig, Germany.

13 *Correspondence to:* Rodrigo Jimenez (rjimenezp@unal.edu.co)

14 **Abstract.**

15 Agro-industrial areas are frequently affected by various sources of atmospheric pollutants that have a negative impact on public
16 health and ecosystems. However, air quality in these areas is infrequently monitored because of their smaller population
17 compared to large cities, especially in developing countries. The Cauca River Valley (CRV) is an agro-industrial region in
18 Southwest Colombia, where a large fraction of the area is devoted to sugarcane and derivative production. The CRV is also
19 affected by road traffic and industrial emissions. This study aims to elucidate the chemical composition of particulate matter
20 fine mode (PM_{2.5}) and to identify the main pollutant sources before source attribution. A sampling campaign was carried out
21 at a representative site in the CRV region, where daily-averaged mass concentrations of PM_{2.5} and the concentrations of water-
22 soluble ions, trace metals, organic and elemental carbon, and various fractions of organic compounds (carbohydrates, n-
23 alkanes, and polycyclic aromatic hydrocarbons – PAHs) were measured. The mean PM_{2.5} was $14.4 \pm 4.4 \mu\text{g m}^{-3}$, and the most
24 abundant constituent was organic material ($52.7\% \pm 18.4\%$), followed by sulfate ($12.7\% \pm 2.8\%$), and elemental carbon (7.1%
25 $\pm 2.5\%$), which indicates secondary aerosol formation and incomplete combustion. Levoglucosan was present in all samples
26 with a mean concentration of ($113.8 \pm 147.2 \text{ ng m}^{-3}$) revealing biomass burning as a persistent source. Mass closure using the
27 EC tracer method explained 88.4% of PM_{2.5}, whereas the organic tracer method explained 70.9% of PM_{2.5}. We attribute this
28 difference to the lack of information of specific organic tracers for some sources, both primary and secondary. Organic material
29 and inorganic ions were the dominant groups of species (79% of PM_{2.5}). OM_{prim} and OM_{sec} contribute 24.2% and 28.5% to

30 PM_{2.5}. Inorganic ions as sulfate, nitrate and ammonia constitute 19.0%; EC, 7.1%; dust, 3.5%; PBW, 5.3%; and TEO, 0.9% of
31 PM_{2.5}. The aerosol was acidic, with a pH of 2.5 ± 0.4 , mainly because of the abundance of organic and sulfur compounds.
32 Diagnostic ratios and tracer concentrations indicate that most PM_{2.5} was emitted locally and had contributions of both
33 pyrogenic and petrogenic sources, that biomass burning was ubiquitous during the sampling period and was the main source
34 of PAHs, and that the relatively low PM_{2.5} concentrations and mutagenic potentials are consistent with low-intensity, year-
35 long Biomass Burning (BB) and sugarcane pre-harvest burning in CRV.

36

37

38 Keywords: agro-industry; pre-harvest burning; PM_{2.5}; chemical speciation; Northern South America

39

40 1. Introduction

41 Urban and suburban locations, with moderate to high population densities, are exposed to air pollutant emissions, including of
42 fine particulate matter (PM) from industry, road traffic, and other anthropogenic activities. Suburban areas may also be
43 impacted by emissions from agricultural activities (Begam et al., 2016). Air quality in areas under these conditions is
44 infrequently monitored, particularly in developing countries, despite the extensive use of highly emitting practices, including
45 intensive use of insecticides and pesticides, fire for land and crop management, and diesel-based mechanization (Aneja et al.,
46 2008, 2009). Agricultural sources emit pollutants, such as volatile organic compounds (VOC), which are precursors of
47 tropospheric ozone (Majra, 2011) and secondary organic aerosols (SOA) (Majra, 2011). Most agricultural activities also emit
48 PM_{2.5} (solid and liquid particles with aerodynamic diameters smaller than 2.5 μm), which may contain black carbon (BC) and
49 toxic and carcinogenic pollutants, e.g., polycyclic aromatic hydrocarbons (PAHs). Other agricultural activities, including
50 mechanized land preparation, sowing and harvesting, consume significant volumes of fossil fuels, particularly diesel, and emit
51 trace gases (including CO₂, CO, SO₂, NO_x, NH₃, VOC) that also generate O₃ and SOA, all of which affect human health and
52 climate (Yadav and Devi, 2019). Furthermore, agricultural operations are a significant source of nitrogen-containing trace
53 gases (NO₂, NO, NH₃, N₂O) that are released from fertilizers, livestock waste, and farm machinery into the atmosphere (Sutton
54 et al., 2011). Also, poultry and pig farming are high emitters of sulfur compounds, particularly H₂S.

55

56 The Cauca River Valley (CRV) is an inter-Andean valley in Southwest Colombia with a flat area of 5287 km² (248 km long
57 by 22 km mean width), a mean altitude of 985 m MSL (Figure 1). CRV is bounded by the Colombian Andes Western and
58 Central Cordilleras and is located at ~120 km from the Pacific Ocean. CRV encompasses the cities of Cali, Colombia's third-
59 largest city with 2.2 million inhabitants (inhab), Yumbo (129 thousand inhab), an important industrial hub, and Palmira (313
60 thousand inhab), an important agro-industry center. Industry is also present in the other major CRV cities (Tuluá, Cartago,
61 Jamundí, and Buga).

62

63 CRV hosts a highly efficient, resource-intensive sugarcane agro-industry with one of the highest biomass yields (up to 120 ton
64 ha⁻¹) and the highest sugar productivities in the world (~13 ton sugar ha⁻¹) (Asocaña, 2018, 2019). Sugarcane sowing,
65 harvesting, and transport to mills are all mechanized and use diesel as fuel. Besides, all the sugarcane bagasse is used, either
66 to produce heat and electric power (cogeneration) or as feedstock to the local paper industry. Moreover, although pre-harvest
67 burning is being phased out in CRV, one-third of the sugarcane area in 2018 was burned prior to harvesting. CRV is also the
68 third largest poultry producer (351,104 ton yr⁻¹), and the first egg producer (4,559 million units per year) in Colombia
69 (Min.Agricultura, 2020). In addition, CRV produces 15.1% of Colombia's pork meat (over 1 million pigs in stock)
70 (Min.Agricultura, 2019) and 1.8% of national beef production (467,782 heads in stock) (Min.Agricultura, 2018). Poultry and
71 livestock production are significant sources of H₂S and NH₃. Besides a long-time established energy-intensive industry, there
72 are also a variety of smaller industries, including brick kilns. Regarding mobile sources, there are nearly 2 million vehicles
73 (1,951,638 vehicles) registered in CRV (RUNT, 2021). These include the standard urban categories along with off-road
74 unregulated farming machinery. The sugarcane agroindustry uses multi-car trailers towed by diesel-powered tractors, with
75 enough annual activity to be considered an independent source (the activity of which is proportional to the sugarcane harvested
76 area and the distance to sugar mills). Overall, CRV mobile sources consumed 772 million L of gasoline and 590 million L of
77 diesel in 2018 (SICOM, 2018). Moreover, the local airport, the most important in southwest Colombia, located very close to
78 Palmira, handled 1.3 million passengers in 2019 (Aerocivil, 2019). Also, 1657 ha of sugarcane and corn were fumigated in
79 2020 using small aircraft (Aerocivil, 2020).

80

81 For this research, we prepared a preliminary, aggregated PM₁₀ emission inventory for CRV by putting together disparate source
82 data, including from the stationary source emission inventories of CRV's six largest cities (Cali, Tuluá, Cartago, Jamundí,
83 Palmira, Yumbo and Buga), Cali's and other cities' mobile source emission inventories, and our estimation of sugarcane pre-
84 harvest burning (PHB) and other point, linear and area sources (Table S1). Our preliminary inventory indicates that the
85 manufacturing industry is by far the main PM₁₀ emitter in CRV, with annual emissions of ~8.2 Gg PM₁₀. PM₁₀ emissions from
86 mobile sources (~1.4 Gg PM₁₀ yr⁻¹) and open-field sugarcane pre-harvest burning (1.7 Gg PM₁₀ yr⁻¹) are a factor ~5 smaller.
87 The emissions of inorganic and organic secondary aerosol precursors are also significant. We estimate that 30.1 Gg of SO₂ are
88 annually emitted in CRV (41% from sugar mills and other agroindustries, 32% from food industries, and 9% from cement,
89 ceramic and asphalt production). Emissions of volatile organic compounds (VOCs) are very similar (34.7 Gg yr⁻¹). Although
90 a significant number of coal-fired boilers have been converted to natural gas, CRV's sulfur-rich coal (1.4-4% total S) is still
91 an important industrial fuel. It must be stressed that this is a preliminary, not fully updated, regional inventory. The available
92 information was insufficient for disaggregating the fine-mode particulate matter emissions (PM_{2.5}). The multiplicity, disparity,
93 and uncertainty of sources are indicative of the complexity of the PM_{2.5} source identification, quantification, and location tasks.

94

95 The particulate matter chemical composition has been widely used for apportionment of pollutant sources and toxicity exposure
96 analyses. Most field measurement-based studies have been conducted in North America, Europe, and Asia (Karagulian et al.,
97 2015). The number of studies in Latin America and the Caribbean (LAC) is much smaller and have focused on the chemical
98 composition of PM_{10} (Pereira et al., 2019; Vasconcellos et al., 2011), as well as the PM source apportionment in urban areas
99 of Colombia (Ramírez et al., 2018; Vargas et al., 2012), Chile (Jorquera and Barraza, 2012, 2013; Villalobos et al., 2015),
100 Costa Rica (Murillo et al., 2013) and Brazil (de Andrade et al., 2010). The number of studies that involve agro-industrial
101 sources and their impact on suburban areas is even smaller. These include the Indo-Gangetic plain (Alvi et al., 2020), the Sao
102 Paulo State in Brazil (Gonçalves et al., 2016; Urban et al., 2016), Ouagadougou in Burkina Faso (Boman et al., 2009), the
103 Anhui Province in China (Li et al., 2014), for which the chemical composition of $PM_{2.5}$ and some of its sources have been
104 identified. Likewise, regions in South America with sugarcane agroindustry, such as Mexico (Mugica-Alvarez et al., 2015;
105 Mugica-Álvarez et al., 2016, 2018) and Brazil (de Andrade et al., 2010; De Assuncao et al., 2014; Lara et al., 2005; Pereira et
106 al., 2017) have also reported on their agroindustry impact on $PM_{2.5}$ levels at nearby population centers. They are very few
107 studies on air pollution in agro-industrial areas of Colombia. Most notably, Romero et al., (2013) measured PAHs and metals
108 in PM_{10} . Most of the studies above identified biomass burning and fossil fuel combustion as significant PM sources, and some
109 also identified industrial and fertilizer use as relevant.

110

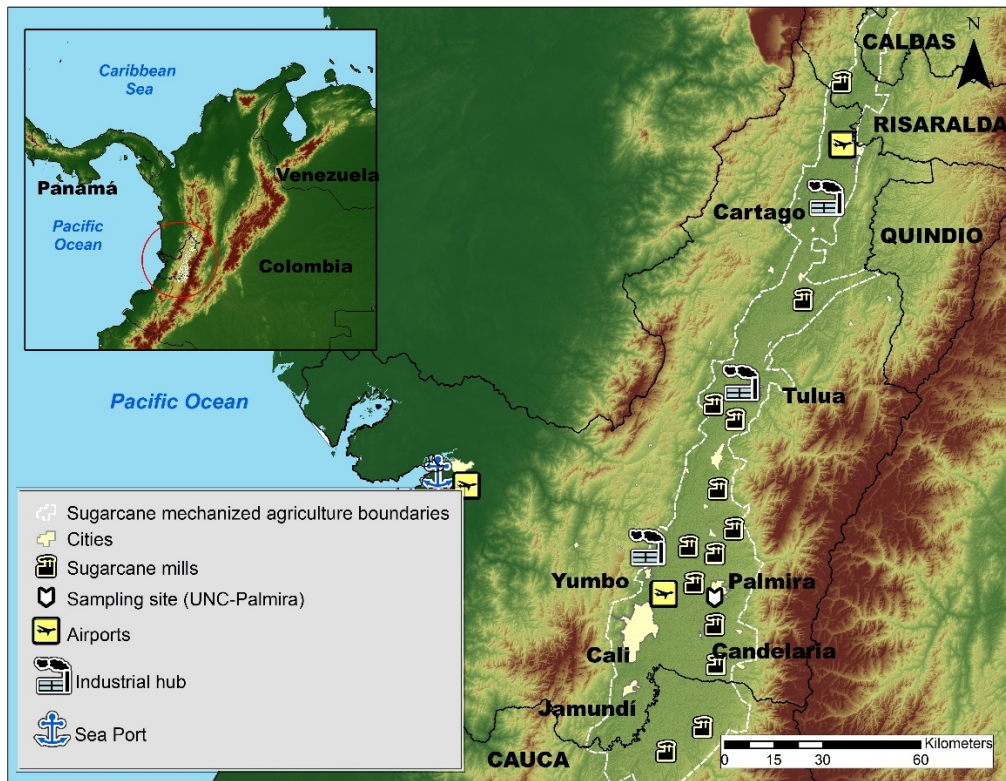
111 This research aimed to characterize the chemical composition of $PM_{2.5}$ at a CRV representative location, including EC, primary
112 and secondary OC, ions, trace metals, and specific molecular markers, such as PAHs, n-alkanes, and carbohydrates, as well as
113 the relationships among these components and with emission sources. Diagnostic ratios were used to identify the most
114 important $PM_{2.5}$ components and as a tool for preliminary pollutant source attribution, including primary and secondary
115 aerosols generated by or associated with sugarcane pre-harvest burning. We believe that in the CRV case, this analysis is
116 needed prior to source apportionment with receptor models for three reasons: 1) This is the first comprehensive investigation
117 of PM composition in the CRV (prior studies included two types of components at most); 2) There are no suitable chemical
118 profiles for some pollutant sources, particularly sugarcane PHB; 3) Our measurement dataset is barely large enough for profile-
119 free receptor modeling (positive matrix factorization). We expect that this study also motivates future research on source
120 apportionment in the region. Our results are particularly relevant for urban communities and atmospheres impacted by large-
121 scale intensive agriculture and industrial emissions, particularly in developing countries, especially in Latin America where
122 PM composition information is still scarce (Liang et al., 2016).

123

124 **2. Methods**

125 **2.1. Description of the sampling site**

126 The sampling site was located on the rooftop of an 8-story administrative building at the Palmira Campus of Universidad
127 Nacional de Colombia (3°30'44.26" N; 76°18'27.40" W, 1065 m altitude), about 27 m above the ground. The campus is located
128 on the western outskirts of Palmira's urban area and is surrounded by short buildings on the east, and extensive sugarcane
129 plantations, several sugar mills, and other industries elsewhere. Palmira is located at ~27 km northeast of Cali and ~22 km
130 southeast of Yumbo, an important industrial hub. The Pacific Ocean coastline stretches at ~120 km across the Western
131 Cordillera, as shown in Figure 1, where operates one of the busiest international trade seaports in Colombia (López, 2017).
132 Most of the freight is transported by diesel-powered trucks. Road traffic is also substantial within the CRV, with Bogota and
133 along the Pan-American highway that connects Colombia with other South American countries (Orozco et al., 2012).



134
135 Figure 1. Map of the Cauca River Valley (CRV). The inset shows the location of CRV in Colombia and in Northern South
136 America. The map shows the main cities in CRV, including Palmira (312 thousand inhabitants), our measurement site, Cali,
137 the largest city in the southwest of Colombia, Yumbo, an industrial hub, and the main highways. Sugar mills, which produce

138 sugar, bioethanol, and electric power are also shown. The dashed-line defined area is CRV's flattest (slope < 5%) bottomland,
139 where mechanized, intensive sugarcane agriculture takes place. Significant diesel combustion emissions occur along the
140 Buenaventura highway because it is one of the busiest ports in Colombia.

141

142 The Andes Cordillera splits into three south-to-north diverging mountain ranges (Western, Central, and Eastern Cordilleras)
143 near the Colombia-Ecuador border (see Figure 1). The Western Cordillera separates the CRV from the Colombian Pacific
144 Ocean watershed, the rainiest region on Earth (Hernández and Mesa, 2020) The elevated precipitation in this basin (Mesa and
145 Rojo, 2020) is due to the presence of a Walker cell convergence zone at the surface, persistent under neutral and La Niña
146 conditions. This synoptic feature is one of the most important determinants of atmospheric circulation in Colombia, with
147 prevailing east-to-west winds in the lower troposphere along with upper troposphere return winds (Mesa and Rojo, 2020). The
148 Andean Cordilleras are nevertheless effective barriers to the Walker circulation near the CRV surface (Lopez and Howell,
149 1967; Mesa S. and Rojo H., 2020). The elevated humidity in the Pacific Ocean watershed and the closeness of the two Andes
150 branches drive a zonal regional circulation pattern, consisting of west-to-east anabatic winds over the Pacific slope of the
151 Western Cordillera during the daytime followed by rapid katabatic winds in the late afternoon (Lopez and Howell, 1967).
152 These winds rapidly ventilate the CRV during the late afternoon – early evening period on an almost regular basis. CRV is
153 wide (~22 km) and long (~248 km) enough to develop a valley-mountain wind circulation pattern during the daytime. Winds
154 are very mild during this time period and expected to be highly dispersive, i.e., with high turbulence intensities (Ortiz et al.,
155 2019). The arrival of the katabatic “tide” in the late afternoon wipes the valley-mountain wind pattern out (Lopez and Howell,
156 1967).

157 **2.2. Sampling protocols**

158 The sampling campaign was conducted between July 25th and September 19th, 2018. PM_{2.5} aerosol particles (aerodynamic
159 diameter < 2.5 μm) were collected on Teflon and quartz fiber filters simultaneously for 23 h (from 12:00 local time – LT – to
160 the next day at 11:00 LT), using 2 in-tandem low-volume samplers (ChemComb speciation samplers, R&P). Each sampler
161 used an independent pump set at a flow rate of 14 L min⁻¹. For both types of filters, three lab blank filters without exposure
162 were analyzed. Quartz filters were pre-baked at 600 °C for 8 h before sampling to eliminate contaminant trace hydrocarbons.
163 In total, 45 samples were collected. Prior to and after exposure, the filters were conditioned at constant humidity (36±1.5%
164 relative humidity) and temperature (24 ± 1.2 °C) for 24 h before being weighing on a microbalance (Sartorius, Mettler Toledo)
165 with a 199.99 g capacity and 10 μg resolution. PM_{2.5}-loaded filters were saved at Petri boxes previously prepared to avoid
166 cross-contamination of organic species. The filters were subsequently stored at –20°C until analysis to reduce the volatilization
167 of species such as ammonium nitrate and semi-volatile organic compounds. Blank quartz filters were pre-baked and stored
168 following an identical procedure to exposed filters to collect samples. Blank Teflon filters were treated under the same
169 conditions of storage, transport, and analysis as PM_{2.5}-loaded filters.

170 Several frequent challenges can affect the PM composition measurements, including the following: 1) Absorption of some
171 gases on the inlet's galvanic steel, which may alter the gas-particle balance of the $\text{HNO}_3 \rightleftharpoons \text{NO}_3^-$ system on the collected PM.
172 No denuders were utilized during the collecting of the samples for this study; 2) Significant temperature changes during
173 sampling, and then during their conditioning before filter weighing may cause ammonium nitrate to volatilize. Because the
174 samples were collected at temperatures ranging from 17 to 33 °C, and then conditioned to 25 °C, shift in the equilibrium of
175 the $\text{HNO}_3 \rightleftharpoons \text{NO}_3^-$ system could have been a source of uncertainty in our data. The vaporization of some semi-volatile organic
176 species throughout the sampling and storage period, as well as the absorption of organic gases in the filter material, are two
177 additional sources of uncertainty.

178 By differential weighing, mass concentrations were determined from the Teflon filters. It is worth mentioning that during the
179 sampling period, 1888 sugarcane PHB events occurred. This information was kindly provided by the regional environmental
180 authority (CVC), from reports by sugarcane producers. The vast majority of these events were intentional, controlled, size-
181 limited (~6 ha median area), and brief (~25 minutes median duration) (Fig S1).

182 **2.3. Analytical methods**

183 The quartz-fiber filter samples were analyzed for ions, metals, elemental and organic carbon, and speciation of the
184 carbonaceous fraction. The Teflon-membrane filter samples were analyzed for metals.

185

186 Two circular pieces with an 8 mm diameter (100.5 mm²) were punched from each quartz and Teflon filter, following the
187 method described by Wadinga Fomba et al., (2020), and extracted using 1 mL of ultrapure water (18 MΩ) in a shaker at 400
188 rpm for 120 min. The extracts were filtered through 0.45 μm syringe filters (Acrodisc Pall). An aliquot of the solution was
189 analyzed for inorganic (K^+ , Na^+ , NH_4^+ , Mg^{2+} , Ca^{2+} , Cl^- , NO_3^- , SO_4^{2-} , NO_2^- , PO_4^{3-} , Br^- , F^-) and some organic ions ($\text{C}_2\text{O}_4^{2-}$,
190 $\text{CH}_3\text{O}_3\text{S}^-$, and CHO_2^-) by ion chromatography (IC690 Metrohm; ICS3000, Dionex). Another aliquot was analyzed for
191 carbohydrates, including levoglucosan, mannosan, and galactosan, as described by Iinuma et al. (2009a). Organic and
192 elemental carbon were determined from 90.0 mm² filter pieces following the EUSAAR 2 protocol (Cavalli et al., 2010), with
193 a thermal-optical method using a Sunset Laboratory dual carbonaceous analyzer.

194

195 Seventeen metals, including K, Ca, Ti, V, Cr, Mn, Fe, Ni, Cu, As, Se, Sr, Ba, Pb, Sn, Sb, and Cu, were analyzed from Teflon
196 (22 samples) and quartz (23 samples) filters by total reflection X-Ray Fluorescence Spectroscopy – TXRF (TXRF, PICOFOX
197 S2, Bruker). Si was not determined as this element is part of the quartz filter substrate. Metals were analyzed from three 8-mm
198 circular pieces punched from Teflon filters, which were digested a nitric and chloride acid solution for 180 min at 180 °C.
199 After this, 20-μl aliquots of the digested solution were placed on the surface of polished TXRF quartz substrates along with
200 10 μl of Ga solution, which served as an internal standard. This solution was left to evaporate at 100°C. The samples were

201 measured at two angles with a difference of 90° between them to ensure complete excitation of metals. More details on the
202 analytical technique can be found in Fomba et al. (2013).

203

204 Alkanes and PAHs were determined from two circular filter punches (6 mm diameter, 56.5 mm²), using a Curie-point pyrolyzer
205 (JPS-350, JAI) coupled to a GC-MS system (6890 N GC, 5973inert MSD, Agilent Technologies). The chemical identification
206 and quantification of the C₂₀ to C₃₄ n-alkanes, as well as the following organic species were performed using the following
207 external standards (Campro, Germany): pristane, phytane, fluorene (FLE), phenanthrene (PHEN), anthracene (ANT),
208 fluoranthene (FLT), pyrene (PYR), retene (RET), benzo(b)naphtho(1,2-d)thiophene (BNT(2,1)), cyclopenta(c,d)pyrene
209 (CPY), benz(a)anthracene (BaA), chrysene(+Triphenylene) (CHRY), 2,2-binaphthyl (BNT(2,2)), benzo(b)fluoranthene (BbF),
210 benzo(k)fluoranthene (BkF), benzo(e)pyrene (BeP), benzo(a)pyrene (BaP), indeno (1,2,3-c,d)pyrene (IcdP),
211 dibenz(a,h)anthracene (DahA), and benzo(g,h,i)perylene (BghiP), coronene (COR), 9H-Fluorenone (FLO(9H)), 9,10-
212 Anthracenedione (ANT (9,10)) and 1,2-Benzanthraquinone (BAQ (1,2)). Four deuterated PAHs, (acenaphthene-d10,
213 phenanthrene-d10, chrysene-d12, and perylene-d12), and two deuterated alkanes (tetracosane-d50 and tetratriacontane-d70)
214 were used as internal standards, following the analytical method described by (Neusüss et al., 2000). For each analyzed
215 compound, the sample concentration was calculated by subtracting the average concentration of three blank filters from the
216 measured concentration.

217 **2.4. Diagnostic ratios and mass closure**

218 The main PM_{2.5} components, organic material (OM), elemental carbon (EC), sulfate, ammonium and nitrate, crustal material
219 (dust), other trace elements oxides (TEOs), and particle-bounded water (PBW), were estimated from the concentrations of EC,
220 OC, water-soluble ions (NO₃⁻, SO₄²⁻ and NH₄⁺), and tracer metal concentrations (Ca, Ti, Fe, Ni, Cu, Zn, As, Se, Sb, Ba, and
221 Pb). PM_{2.5} closure is described by Eq 1 (Dabek-Zlotorzynska et al., 2011). We used the Interagency Monitoring of Protected
222 Visual Environment (IMPROVE) equations (Chow et al., 2015) to quantify the concentrations of main compounds (Table 1).
223 The aerosol particle bounded water content was estimated from the measured ionic composition, relative humidity, and
224 temperature, following the aerosol inorganic model (AIM) described by (Clegg et al., 1998), which is available for running
225 online at <http://www.aim.env.uea.ac.uk/aim/model2/model2a.php>. The thermodynamic equilibrium of the system H⁺- NH₄⁺ -
226 Na⁺ - SO₄²⁻ - NO₃⁻ - Cl⁻ - H₂O was described by and estimated from AIM.

227

$$228 \quad PM_{2.5}(\text{mass closure estimated}) = OM_{pri} + OM_{sec} + EC + SO_4^{2-} + NH_4^+ + NO_3^- + Dust + TEO + PBW \quad \text{Eq (1)}$$

Component	Equation	Reference
OM _{prim}	$= f_1 \text{ OC}_{\text{prim}}$	(Chow et al., 2015) (Turpin and Lim, 2010)
OM _{sec}	$= f_2 \text{ OC}_{\text{sec}}$	(El-Zanan et al., 2005)
SO ₄	$= \text{SO}_4^{2-}$	(Chow et al., 2015)
NO ₃	$= \text{NO}_3^-$	(Chow et al., 2015)
NH ₄ ⁺	$= \text{NH}_4^+$	(Chow et al., 2015)
Dust	$= 1.63\text{Ca} + 1.94\text{Ti} + 2.42\text{Fe}$ (Assuming CaO, Fe ₂ O ₃ , FeO (in equal amounts) and TiO ₂)	(Chow et al., 2015)
PBW	$= k (\text{SO}_4^{2-} + \text{NH}_4^+)$	(Clegg et al., 1998)
TEO	$= 1.47[\text{V}] + 1.27[\text{Ni}] + 1.25[\text{Cu}] + 1.24[\text{Zn}] + 1.32[\text{As}] +$ $1.2[\text{Se}] + 1.07[\text{Ag}] + 1.14[\text{Cd}] + 1.2[\text{Sb}] + 1.12[\text{Ba}] +$ $1.23[\text{Ce}] + 1.08[\text{Pb}]$	(Snider et al., 2016)

230 $f_1 = 1.6$. This factor was estimated considering the predominant sources.

231 $f_2 = 2.1$. This factor was estimated by subtracting the non-carbon component of PM_{2.5} from the measured mass.

232 $k = 0.32$ was calculated using the Aerosol Inorganic Model.

233

234 The EC tracer method was applied to estimate primary (OC_{prim}) and secondary (OC_{sec}) organic carbon (Lee et al., 2010). This

235 method utilizes EC as a tracer for primary OC, which implies that OC_{prim} from non-combustion sources is deemed negligible.

236 Primary and secondary OC can be estimated by defining a suitable primary OC to EC ratio ([OC/EC]_{prim}). See Eq (2) and Eq

237 (3). We estimated the [OC/EC]_{prim} ratio as the slope of the Deming linear fit between EC and OC measurements. The term b

238 corresponds to the linear fit intercept, which can be interpreted as the emitted OC_{prim} that is not associated with EC emissions.

239 This method is limited as per the following assumptions: 1) [OC/EC]_{prim} is deemed constant, while in reality it may change

240 throughout the day depending on factors such as wind direction and the location of the dominant emission sources. Our 23-h

241 sampling is expected to smooth this variability source out; 2) It neglects OC_{prim} from non-combustion sources; and 3) It assumes

242 that OC_{prim} is nonvolatile and nonreactive. Departure from these assumptions implies that the estimation of OC_{prim} and OC_{sec}

243 might be biased, likely underestimating OC_{sec}.

244

$$245 \quad \text{OC}_{\text{prim}} = [\text{OC}/\text{EC}]_{\text{min}} * \text{EC} + b \quad \text{Eq (2)}$$

$$246 \quad \text{OC}_{\text{sec}} = \text{OC} - \text{OC}_{\text{prim}} \quad \text{Eq (3)}$$

247 OC_{prim} was also estimated by using an organic tracer method involving three sources considered significant in CRV, namely

248 fossil fuel combustion (OC_{FF}), biomass burning (OC_{BB}), and vegetable detritus (OC_{det}). OC_{FF}, OC_{BB} and OC_{det} were estimated

249 by fitting a linear model (Eq (4) using robust regression (M estimator with bisquare function), which were find the coefficients

250 X, Y and Z to multiply the tracer concentrations of each source. The tracers used were the sum of the BghiP and IcdP for fossil
251 fuel (T_{FF}); levoglucosan for biomass burning (T_{BB}); and the sum of the highest molecular weight alkanes ($C_{27} - C_{33}$) for
252 vegetable detritus (T_{det}). The sum of each tracer multiply by X, Y and Z, respectively, Eq (5), corresponding to OC_{prim} attributed
253 to known sources present in CRV. The subtraction of OC_{prim} attributed to OC total is named OC_{rest} , which corresponding to
254 another sources of OC primary and OC secondary.

$$255 \quad OC_{prim} = (T_{FF} * X) + (T_{BB} * Y) + (T_{det} * Z) \quad \text{Eq (4)}$$

$$256 \quad OC_{prim} = OC_{FF} + OC_{BB} + OC_{det} \quad \text{Eq (5)}$$

$$257 \quad OC_{rest} = OC - OC_{prim} \quad \text{Eq (6)}$$

258 Following Table 1, OM was estimated from OC using the conversion factors f_1 and f_2 (Chow et al., 2015). These are dependent
259 on the OM oxidation level and secondary organic aerosol (SOA) formation and aging during air mass movements. Turpin and
260 Lim (2001a) recommended an OM/OC ratio of 1.6 ± 0.2 for urban aerosols, and 2.1 ± 0.2 for non-urban aerosols. These values
261 are comparable to those reported by Aiken et al. (2008) of 1.71 (1.41 – 2.15), where lower values (1.6 – 1.8) are typical of
262 ground measurements in the morning, and higher values (1.8 – 1.9) of aircraft samples. The conversion factors for BB aerosols
263 can be even higher (2.2-2.6), due to the presence of organic components with higher molecular weights, e.g., levoglucosan.
264 However, Andreae (2019) recommends a factor of 1.6 for fresh BB aerosol, which is consistent with Hodshire et al (2019).
265 We believe that traffic and biomass burning are the dominant primary OC sources at our site. Therefore, we used $f_1 = 1.6$ to
266 estimate OM_{pri} , and $f_2 = 2.1$ to estimate OM_{sec} from the OC_{sec} . This factor was chosen based on recommended ratios of 2.1 ± 0.2
267 for aged aerosols (Schauer, 1998). It is worth mentioning that some global climate models estimate direct radiative forcing
268 from organic material present in aerosols using OM/OC ratios without separating sources, while others apply different ratios
269 depending on type of source, particularly values ranging within 1.4 - 1.6 for fossil fuels and biofuel, and 2.6 for biomass
270 burning. Other models use specific molecules as tracers of OM, such as monoterpenes, isoprene, aromatics and alkanes.
271 Tsigaridis et al., (2014) present a list of tracers than haven been used in various models to quantify OM in the aerosols.

272

273 Concentration ratios among distinct species were used to chemically characterize and infer the main sources of fine particle
274 matter at Palmira. The cation/anion equivalent ratio and the $[NH_4^+]/[SO_4^{2-}]$ molar ratio were used as preliminary proxies for
275 $PM_{2.5}$ acidity. The first one is based on electroneutrality and assumes that H^+ balances out the excess of anions in the solution.
276 The cation equivalent to anion equivalent ratio was calculated using Eq (7) and Eq (8) for each term. The second ratio is an
277 indicator of acidity attributable to those two ions, which are usually the most abundant among cations and anions in $PM_{2.5}$.

278

279 However, these approaches to inferring the $PM_{2.5}$ acidity can result in challenging interpretations, incomplete and incorrect
280 results due to an indirect connection to the system's acidity (Pye et al., 2020). Therefore, the E-AIM (Extended Aerosol

281 Inorganics Model) was used to estimate the equilibrium state of a system containing water and the following : SO_4^{2-} , NH_4^+ ,
 282 NO_3^- , Na^+ and Cl^- ions, in equilibrium with an atmosphere at known temperature and relative humidity but without information
 283 on gas-phase concentrations (NH_3 , HNO_3 and SO_2), as these were not available in our investigation. The H^+ mole fraction
 284 concentration from E-AIM IV (Friese and Ebel, 2010), was used to calculate pH following Eq (9). E-AIM requires that the
 285 input data for ionic composition to be balanced on an equivalent basis, which means that the sums of the charges on the cations
 286 and anions considered in the system do balance, accordingly $[\text{SO}_4^{2-}] + [\text{NO}_3^-] + [\text{Cl}^-] = [\text{NH}_4^+] + [\text{Na}^+]$. The disadvantage of
 287 this approach is that it does not allow for the partitioning of trace gases into the vapor phase (the model is available at
 288 <http://www.aim.env.uea.ac.uk/aim/model4/model4a.php>; last access 2022-01-22).

289

$$290 \quad AE = \frac{[\text{SO}_4^{2-}]}{48} + \frac{[\text{NO}_3^-]}{62} + \frac{[\text{C}_2\text{O}_4^{2-}]}{44} + \frac{[\text{Cl}^-]}{35} + \frac{[\text{PO}_4^{3-}]}{31.3} + \frac{[\text{NO}_2^-]}{46} + \frac{[\text{Br}^-]}{79.9} + \frac{[\text{F}^-]}{18.9} + \frac{[\text{CH}_3\text{O}_3\text{S}^-]}{95} + \frac{[\text{CHO}_2^-]}{45} \quad \text{Eq (7)}$$

$$291 \quad CE = \frac{[\text{Na}^+]}{23} + \frac{[\text{K}^+]}{39} + \frac{[\text{NH}_4^+]}{18} + \frac{[\text{Mg}^{2+}]}{12} + \frac{[\text{Ca}^{2+}]}{20} \quad \text{Eq (8)}$$

$$292 \quad \text{pH}_x = -\log_{10}(\text{H}^+) \quad \text{Eq (9)}$$

293

294 Parent PAH ratios are widely used to identify combustion-derived PAHs (Khedidji et al., 2020; Szabó et al., 2015; Tobiszewski
 295 and Namieśnik, 2012), although some of them are photochemically degraded in the atmosphere (Yunker et al., 2002).
 296 Additionally, n-alkanes are employed as markers of fossil fuel or vegetation contributions to $\text{PM}_{2.5}$. Carbon number maximum
 297 concentration (C_{max}), carbon preference index (CPI), and wax n-alkanes percentage (WNA%) were the criteria utilized to
 298 determine n-alkane origin. Table 2 summarizes the diagnostic ratio equations and the expected dominating source based on
 299 ratio values.

300

301 Table 2. Diagnostic ratios of organic compounds used to infer the sources of PM_{2.5} in this study.

Diagnostic ratios	Equation	Value	Source	References
BeP/(BeP+BaP)		~0.5 < 0.5	Fresh particles Photolysis	(Tobiszewski and Namieśnik, 2012)
IcdP/(IcdP+BghiP)		<0.2 0.2 - 0.5 >0.5	Petrogenic Petroleum combustion Grass, wood and coal combustion	(Yunker et al., 2002) (Tobiszewski and Namieśnik, 2012)
BaP/BghiP		<0.6 >0.6	Non-traffic emissions Traffic emissions	(Tobiszewski and Namieśnik, 2012) (Szabó et al., 2015)
IcdP/BghiP		>1.25 <0.4	Brown coal* Gasoline	(Ravindra et al., 2008)
LMW/(MMW+HMW)		<1 >1	Pyrogenic Petrogenic	(Tobiszewski and Namieśnik, 2012)
C _{max}		< C ₂₅ C ₂₇ - C ₃₄	Anthropogenic Vegetative detritus	(Lin et al., 2010)
CPI	$CPI = 0.5 * \left[\frac{\sum_{19}^{33} C_i}{\sum_{20}^{32} C_k} + \frac{\sum_{19}^{33} C_i}{\sum_{22}^{34} C_k} \right]$	CPI ~1 CPI > 1	Fossil carbon Biogenic	(Marzi et al., 1993) (Kang et al., 2018)
WNA%	$\sum WNA_{C_n} = [C_n] - \left[\frac{(C_{n+1}) + (C_{n-1})}{2} \right]$ $WNA\% = \frac{\sum WNA_{C_n}}{\sum Total\ n - alkanes}$ $PNA\% = 100 - WNA\%$	WNA ~ 100 PNA ~ 100	Biogenic Anthropogenic	(Lyu et al., 2019)

*Used for residential heating and industrial operation.

302

303

304 As all measured variables were subject to analytical uncertainty and temporal variability, linear fitting parameters were
 305 obtained from Deming regressions as recommended for atmospheric measurements (Wu and Zhen Yu, 2018). The Spearman
 306 coefficient was selected instead of Pearson's as an indicator of statistical correlation between chemical components to reduce
 307 the effect of outliers. Derived ratios and other parameters were considered statistically significant when p-values < 0.05. The
 308 statistical analysis was conducted using R version 4.0.2, 24 including the packages corr (0.4.2), mcr (1.2.1), cluster (2.1.0),
 309 tidyverse (1.3.0), ggplot (3.3.2), MASS (7.3-53.1) and openair (2.7-4).

310 3. Results and discussions

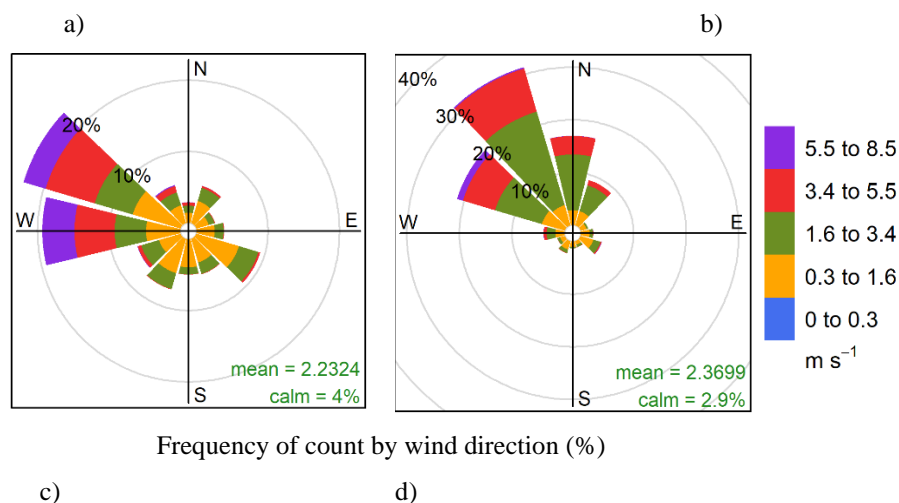
311 3.1. Meteorology

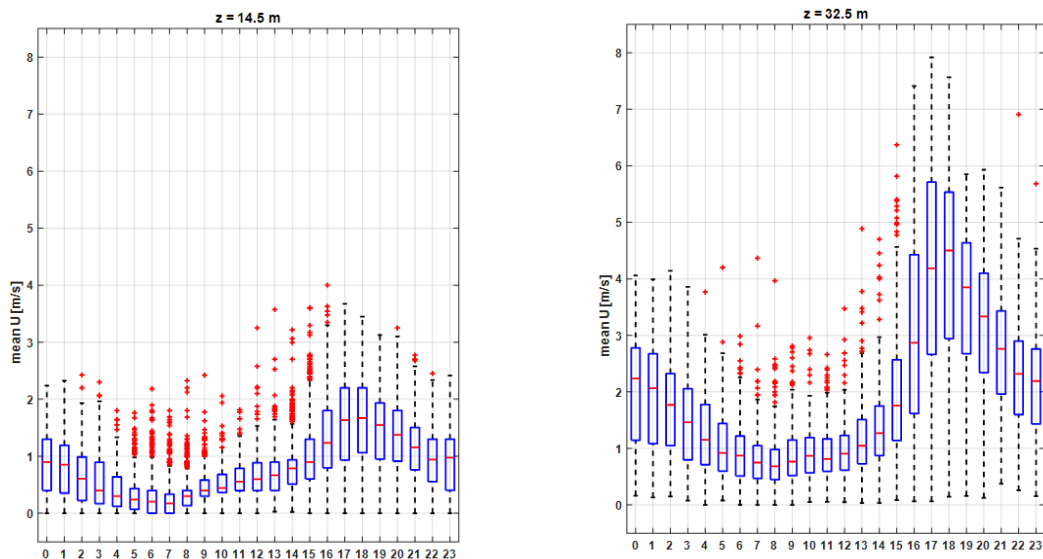
312

313 One year prior to the sampling period, we monitored the local meteorology, first at 14.5 m above the ground, a few meters
 314 over the mean canopy level, and then at 32.5 m above the ground during the sampling campaign. The box-and-whisker plot in

315 Fig 2 shows katabatic tide winds of up to ~8 m/s at the sampling site elevation, peaking at ~17:00 local time (LT). Wind speeds
 316 were a factor ~2-3 slower at ground level. The wind runs at the sampling height were typically above ~200 km per day (Fig
 317 S3) indicating that the samples had substantially broader spatial coverage of the CRV, much larger than it would have been at
 318 ground level. This also implies that the samples were frequently and significantly influenced by emissions coming from
 319 Yumbo's industrial hub (northwest of Palmira), and also by Palmira and Yumbo urban and highway emissions, as well as
 320 sugarcane PHB and sugarcane mill emissions. The wind rose (Fig 2a) suggests that the influence of urban emissions from Cali,
 321 CRV's largest city by far, was minor. Other meteorological variables are reported in the Supplementary Material (SM) (Fig
 322 S2). Temperature (24.2°C on average) and relative humidity (71.6%) were very likely controlled by solar radiation (350 W m⁻²
 323 on average). The late-afternoon katabatic tide is fast enough to temporarily reduce temperature. The daily pressure profile
 324 (~763 hPa on average) clearly showed the influence of the katabatic tide, with a ~3 hPa drop during its arrival in the late
 325 afternoon. Overall, we believe our measurements at the Palmira site are reasonably representative of the regional air quality.

326





327 Figure 2. Wind pattern in the sampling location: a) predominant wind rose during the sampling period (July - September 2018),
 328 b) hourly profile of wind speed at 14.5 m above the ground (August – December 2017), and c) hourly profile of wind speed in
 329 sampling location at 32.5 m over the ground level (December 2017 – September 2018). *Red points corresponding to upper
 330 10% outliers.

331

332 3.2. Bulk PM_{2.5} concentration and composition

333

334 The daily PM_{2.5} concentration measured in this study ranged from 6.73 to 24.45 $\mu\text{g m}^{-3}$ with a campaign average of $14.38 \pm$
 335 $4.35 \mu\text{g m}^{-3}$ (23 h-average, ± 1 -sigma). Although these concentrations may appear comparatively low, it is worth stressing that
 336 samples were collected at more than 30 m height, with hourly wind speeds frequently above 4 m s^{-1} . However, most days
 337 during this study, PM_{2.5} concentration exceeded the 5 $\mu\text{g m}^{-3}$ annual mean and 15 $\mu\text{g m}^{-3}$ 24-h mean guidelines by World Health
 338 Organization, (2021). Nevertheless, the Colombian standards are less demanding, thus observed concentrations comply with
 339 the 37 $\mu\text{g m}^{-3}$ 24-h mean (MADS, 2017).

340

341 Previous studies conducted in rural areas of Brazil impacted by open field sugarcane burning reported significantly higher
 342 (mean 22.7 $\mu\text{g m}^{-3}$; Lara et al., 2005), similar (mean 18 $\mu\text{g m}^{-3}$ Souza et al., 2014), and significantly lower PM_{2.5} concentrations
 343 (mean 10.88 $\mu\text{g m}^{-3}$; Franzin et al., 2020). Comparable measurements in Mexico during harvest periods showed much higher
 344 concentrations, from 29.14 $\mu\text{g m}^{-3}$ (Mugica-Alvarez et al., 2015) up to 51.3 $\mu\text{g m}^{-3}$ (Mugica-Álvarez et al., 2016). Our PM_{2.5}
 345 concentration measurements in the CRV are thus substantially lower than those usually reported in Mexico and Brazil during
 346 sugarcane burning periods. Major differences among sugarcane PHB practices in Colombia, Brazil and Mexico must be

347 considered while comparing concentrations. First, ~1/3 of the sugarcane harvested area is burned before harvest at CRV. This
348 fraction is much larger in Mexico and Brazil (FAO, 2020). Second, sugarcane is harvested year-round in CRV, as opposed to
349 Brazil and Mexico, where harvest is limited to a ~6-month period (known in Spanish as *zafra*, “the harvest”). Third, the size
350 of the individual plots burned in CRV is typically ~6 ha (median burned area; Cardozo-Valencia et al., 2019), compared to
351 much larger plots and total areas in Brazil and Mexico (FAO, 2020).

352

353 OC was the most abundant measured PM_{2.5} component with a mean daily concentration of $3.97 \pm 1.31 \mu\text{g m}^{-3}$, whereas the
354 mean EC concentration was only $0.96 \pm 0.31 \mu\text{g m}^{-3}$. These two components contributed to $29.1 \pm 8.3\%$ and $7.2 \pm 2.3\%$ of the
355 PM_{2.5} mass, respectively (carbonaceous fractions were thus $4.93 \pm 1.58 \mu\text{g m}^{-3}$, i.e. $36.31 \pm 10.41\%$ of PM_{2.5}).

356

357 The most abundant water-soluble ions found in Palmira’s PM_{2.5} were SO₄²⁻, NH₄⁺, and NO₃⁻, with average concentrations of
358 $2.15 \pm 1.39 \mu\text{g m}^{-3}$, $0.67 \pm 0.62 \mu\text{g m}^{-3}$, and $0.51 \pm 0.30 \mu\text{g m}^{-3}$, respectively ($12.7 \pm 2.8\%$, $3.7 \pm 1.1\%$ and $2.6 \pm 1.3\%$ of mass
359 concentration, respectively). Other water-soluble ions, such as Na⁺, Ca⁺, and C₂O₄²⁻, had mean concentrations of around 0.1
360 $\mu\text{g m}^{-3}$, while those of K⁺, PO₄³⁻, CH₃O₃S⁻, Mg²⁺, and Cl⁻ had concentrations ranging from 10-80 ng m⁻³ (Table 3).

361

362 The predominant elements were Ca ($0.42 \pm 0.33 \mu\text{g m}^{-3}$), K ($0.13 \pm 0.08 \mu\text{g m}^{-3}$), and Fe ($88 \pm 65 \text{ ng m}^{-3}$), followed by Zn (34
363 $\pm 33 \text{ ng m}^{-3}$), Pb ($18 \pm 19 \text{ ng m}^{-3}$), Sn ($52 \pm 37 \text{ ng m}^{-3}$), Ti ($5 \pm 4 \text{ ng m}^{-3}$), Ba ($9 \pm 13 \text{ ng m}^{-3}$), Sr ($2 \pm 5 \text{ ng m}^{-3}$). Mn, Ni, Cr, and
364 Se concentrations were below $2 \pm 1 \text{ ng m}^{-3}$. Trace metals such as Ti, Cr, Mn, K, Ca, Fe, Ni, Cu, Zn Sr, Pb and Se were found
365 in all PM_{2.5} samples, while V was found only in a few samples. Other trace metals such as As and Sb were detected only at a
366 reduced number of samples with concentrations below 20 ng m^{-3} . Table 3 shows the mean, standard deviation, minimum, and
367 maximum concentration of the carbonaceous fraction, soluble ions, and metals found in the PM_{2.5} samples collected in the
368 CRV.

369

370

371

372

373

374

375

376

377

378 Table 3. Mean, 1 standard deviation, minimum and maximum concentrations of carbonaceous fraction, soluble ions, and
379 metals in samples of PM_{2.5} collected in Palmira.

Species	# of samples	Mean	SD	Min	Max	Units
PM _{2.5}	22	14.38	4.35	6.73	24.45	μg m ⁻³
OC	45	3.97	1.31	2.31	8.35	
EC	45	0.96	0.31	0.52	2.15	
SO ₄ ⁻²	45	2.15	1.39	0.98	10.27	
NH ₄ ⁺	45	0.67	0.62	0.18	4.29	
NO ₃ ⁻	45	0.51	0.30	0.11	1.45	
Na ⁺	19	0.21	0.16	0.02	0.45	
Ca ⁺² (Water soluble ion)	45	0.14	0.06	0.06	0.28	
C ₂ O ₄ ⁻²	45	0.11	0.06	0.04	0.36	
K ⁺ (Water soluble ion)	45	0.09	0.06	0.02	0.30	
Ca (Trace metal)	42	0.42	0.33	0.01	1.95	
K (Trace metal)	43	0.13	0.08	0.02	0.46	
Formate	13	82	88	0	217	ng m ⁻³
PO ₄ ⁻³	21	66	42	10	148	
Methansulfonate	45	50	36	13	256	
Cl ⁻	30	20	19	0	75	
Mg ⁺²	45	19	10	2	52	
NO ₂ ⁻	45	3	1	1	6	
Fe	42	88	64	2	293	
Sn	23	52	37	9	137	
Zn	42	34	33	0	153	
Pb	42	18	19	0	84	
Ba	20	9	13	2	72	
Sb	19	8	5	3	22	
Cu	42	6	5	1	22	
Ti	42	5	4	0	17	
As	5	2	4	0	10	
Mn	42	2	1	0	5	
Ni	42	2	1	0	9	
Sr	42	2	5	0	28	
Cr	41	1	1	0	4	
Se	41	1	1	0	6	
V	20	0	1	0	3	

380

381

382

383 3.3. Ions

384

385 SO_4^{2-} and NH_4^+ were the most abundant anion and cation in the $\text{PM}_{2.5}$ samples. The molar ratio $[\text{NH}_4^+]/[\text{SO}_4^{2-}]$ was 1.6 ± 0.3
386 (min: 0.8 and max: 2.3), suggesting that $\text{PM}_{2.5}$ is acidic. The pH of $\text{PM}_{2.5}$ samples was determined using the IV E-AIM
387 thermodynamic model, which estimates the activity coefficient of these species in aqueous phase equilibrium using the H^+ -
388 NH_4^+ - Na^+ - SO_4^{2-} - NO_3^- - Cl^- - H_2O system. As a result, the pH was 2.5 ± 0.4 . The correlation between the $[\text{NH}_4^+]/[\text{SO}_4^{2-}]$ ratio and
389 the pH was strong ($r^2 = 0.96$; Figure S3), suggesting that the molar concentrations of these ions significantly explained the
390 particle acidity. Other studies have reported similar $[\text{NH}_4^+]/[\text{SO}_4^{2-}]$ values for pH values lower than the estimated for CRV.
391 For instance, Xue et al., (2011) shows molar ratios in ranging from 1.32 to 1.71 and pH values between -0.45 and 0.59. Pye et
392 al., (2020) showed that fine particles have a bimodal distribution of pH, with one mode around a pH of 1–3, and another mode
393 around a pH of 4–5, the latter influenced by dust, sea spray, and potentially biomass burning. In this study, only one $\text{PM}_{2.5}$
394 sample exceed a pH value of 4. Overall, this is an indicator of the abundance of sulfate and organics compounds in samples
395 collected in CVR.

396

397 pH affects the partitioning of total nitrate ($\text{NO}_3^- + \text{HNO}_3$) and total ammonium ($\text{NH}_4^+ + \text{NH}_3$) between the gas and particulate
398 phases. Lower pH values favor the partitioning of total nitrate toward the gaseous phase (HNO_3) rather than the particulate
399 phase (NO_3^-). In contrast, the partitioning of total ammonium is favored toward the particulate phase, remaining as NH_4^+ in
400 the aerosol, whereas SO_4^{2-} is a nonvolatile species that remained in the particulate phase. Acidity conditions in the samples
401 collected in this study are consistent with concentrations of SO_4^{2-} , NH_4^+ , and NO_3^- , corresponding to $2.5 \mu\text{g m}^{-3}$, $0.7 \mu\text{g m}^{-3}$,
402 and $0.5 \mu\text{g m}^{-3}$, respectively. Ammoniated sulfate and ammonium nitrate are generally considered the predominant forms of
403 nitrate and sulfate in the inorganic fraction in fine particles. In ammonium-limited conditions, ammonia reacts preferentially
404 with H_2SO_4 to form ammonium sulfate ($[\text{NH}_4]_2\text{SO}_4$), letovicite ($[\text{NH}_4]_3\text{H}[\text{SO}_4]_2$) or ammonium bisulfate ($[\text{NH}_4\text{HSO}_4]$) (Lee et
405 al., 2008). Although the correlation coefficient between SO_4^{2-} and NH_4^+ concentrations was high ($R^2 = 0.98$), the amount of
406 ammonium contained in the samples was not high enough to neutralize sulfate completely and form $[\text{NH}_4]_2\text{SO}_4$. In ammonium-
407 limited atmospheres is expected that not completely neutralized sulfate salts form, such as, as $[\text{NH}_4]_3\text{H}[\text{SO}_4]_2$ and $[\text{NH}_4\text{HSO}_4]$
408 (Ianniello et al., 2011). Thus, based on the limited ammonium concentrations found in CRV's $\text{PM}_{2.5}$, and taking into
409 consideration stoichiometric molar ratios $[\text{NH}_4^+]/[\text{SO}_4^{2-}]$ of 3:2 for letovicite and 1:1 for ammonium bisulfate, and the results
410 of the E-AIM model, it is reasonable to assume that a mixture of sulfate salts is present in CRV's $\text{PM}_{2.5}$, such as, ammonium
411 bisulfate, letovicite, and ammonium sulfate, which form progressively, depending on ammonia availability. The E-AIM model
412 indicates the saturation ratio for each solid species, which usually forms before ammonium bisulfate than letovicite and
413 ammonium sulfate. For a molar ratio of 1.5, the aerosol phase consists almost exclusively of letovicite, while to form
414 ammonium sulfate, the ratio should be over 2.0 (Seinfeld and Pandis, 2006). As result of the $[\text{NH}_4^+]/[\text{SO}_4^{2-}]$ ratios observed in

415 the samples collected in CRV and the pH estimated from the IV E-AIM model, there is no reason to assume that nitrate is
416 present as ammonium nitrate in CRV's PM_{2.5}.

417

418 Instead of this, NO₃⁻ might be bound to cations contained in sea salt and dust particles to form relative nonvolatile salts, as
419 KNO₃, NaNO₃ and Ca(NO₃)₂. NO₃⁻ showed correlation with Na⁺, Ca²⁺ and K⁺ (r² = 0.6, 0.2 and 0.2, respectively), indicating
420 possible formation of these salts. The correlation between Na⁺ and NO₃⁻ could be explained by the impact of sea salt aerosol
421 that comes from air mass origin in the Pacific Ocean. However, the amount of Na⁺ is not enough to neutralize the total of NO₃⁻
422, while Ca²⁺ showed to be sufficient to neutralize NO₃⁻. The molar ratio observed in PM_{2.5} samples of CRV for [NO₃⁻]/[Ca²⁺]
423 was 2.6 ± 1.4, [NO₃⁻]/[Na⁺] was 1.7 ± 1.3, and [NO₃⁻]/[K⁺] was 5.0 ± 3.2, overcoming the stoichiometric molar ratio required
424 to form Ca(NO₃)₂, NaNO₃, and KNO₃.

425

426 The abundance of SO₄²⁻ in CRV's PM_{2.5} can be attributed to oxidation of SO₂ and SO₃ emitted by coal- fired boilers and other
427 combustion equipment (Wang et al., 2016), biomass burning activities (Song et al. (2006)), including PHB and bagasse
428 combustion, and the emission of H₂S associated to poultry and pork production (Casey et al., 2006). The H₂S emission from
429 poultry and pork production were estimated using a mean emission factor associated to live animal units (AU) - time housing,
430 where one AU corresponding to 500 kg of body mass. H₂S emissions from swine and poultry housing are usually lower than
431 5 g H₂S AU⁻¹ d⁻¹ Casey et al., (2006). With this emission factor, we estimate these emissions at 3.5 Ton H₂S d⁻¹ due to poultry
432 and 5 Ton H₂S d⁻¹ associated with pork production. Ammonia emissions factors by poultry and livestock vary from 0.09 to
433 12.9 AU⁻¹ d⁻¹, which led to emission of 9.05 ton NH₃ d⁻¹ from poultry and 12 ton d⁻¹ due to pork production.

434

435 PM_{2.5} consistently contained methanesulfonate, with an average concentration of 50 ng ± 13 m-3. This ion is produced by the
436 aqueous oxidation of dimethyl sulfide (DMS), one of the most prevalent biogenic sulfur compounds in the troposphere. DMS
437 oxidation is a major source of non-sea salt sulfate aerosols in marine areas (Tang et al., 2019), but also can have origin in
438 continental origins, such as biomass burning, (Gondwe, 2004; Meinardi et al., 2003; Sorooshian et al., 2015; Stahl et al., 2020).
439 Methanesulfonate was mainly correlated to the ions sulphate and ammonia (r² = 0.88) and C₂O₄²⁻ (r² = 0.66), the metals Se (r²
440 = 0.74) and Fe (r² = 0.41) and the carbonaceous fraction EC (r² = 0.56) and OC (r² = 0.49) in this study. Knowing the origin
441 of this ion in PM_{2.5} in CRV, which is not directly coastal area, prompts future studies with a higher time resolution (6-12 hours)
442 to establish the connection with changes in the wind pattern and the impact of the katabatic circulation, especially because
443 biomass burning, mainly from sugarcane burnt, is an activity developing during all year in CRV .

444

445 The measured average ratio of [SO₄²⁻]/[NO₃⁻] = 4.5 ± 2.9. This ratio is higher than the one obtained by Souza et al. (2014) at
446 Piracicaba (3.6 ± 1.0) and Sao Paulo (1.8 ± 1.0), Brazil. The strong correlations between SO₄²⁻ and NH₄⁺ (r² = 0.84), SO₄²⁻ and
447 methanesulfonate (CH₃O₃S⁻) (r² = 0.88), and SO₄²⁻ and oxalate dianion (C₂O₄²⁻) (r² = 0.71) allow us to infer that inorganic
448 secondary aerosol formation is a significant PM_{2.5} source in the CRV. In addition, the presence of potassium cation (K⁺) in

449 submicron particles is recognized as a biomass burning tracer (Andreae, 1983; Ryu et al., 2004). K^+ showed a moderate
450 correlation with nitrite anion (NO_2^-) ($r^2 = 0.44$) and $C_2O_4^{2-}$ ($r^2=0.43$) in the CRV, which suggests that biomass burning
451 influences secondary aerosol formation. Mg^{2+} and Ca^{2+} ions, usually considered crustal metals, exhibited a moderate
452 correlation of $r^2 = 0.59$ (Li et al., 2013). Also, Mg^{2+} and $C_2O_4^{2-}$ moderate correlation ($r^2 = 0.26$) points to a link between crustal
453 species and secondary aerosols. Such an association could be plausibly explained by soil erosion induced by pyro-convection
454 during sugarcane pre-harvest burning (Wagner et al., 2018). Our study full species correlation matrix is shown in Fig 4S.

455

456 3.4. Metals

457

458 The measured total $PM_{2.5}$ trace metal concentration was $706 \pm 462 \text{ ng m}^{-3}$ (101.3 ng m^{-3} to 2638 ng m^{-3}). Trace metals can
459 originate from non-exhaust and exhaust emissions. Non-exhaust emissions come from brake and tire wear, road surface
460 abrasion, wear/corrosion of other vehicle components, and the resuspension of road surface dust (Pant and Harrison, 2013).
461 Metals in exhaust emissions are related to fuel, lubricant combustion, catalytic converters, and engine corrosion. As shown by
462 Kundu and Stone (2014), many of these sources share some metals in their chemical composition profile, thus an unambiguous
463 specific source attribution is non-trivial. In this study, we found a significant correlation among Fe, Mn and Ti ($r^2 \approx 0.72$),
464 which is typically associated with a high abundance of crustal material (Fomba et al., 2018), indicating that soil dust is a
465 significant source in the CRV. Also, tire and brake wear tracer metals, including Zn and Cu, showed weaker but still significant
466 correlations among them ($r^2 \approx 0.32$). Ca concentrations were quite high ($405 \pm 334 \text{ ng m}^{-3}$ (1.6 ng m^{-3} to 1952 ng m^{-3}). These
467 levels can be attributed to dust generation by agricultural practices, particularly land planning, liming and tilling, PHB pyro-
468 convection-induced soil erosion, and traffic-induced soil resuspension on unpaved rural roads. One of the very few previous
469 investigations into on PM composition in the CRV (Criollo and Daza, 2011) analyzed trace metals in PM_{10} at 4 CRV locations,
470 including same area where was conducted our study. They found significant enrichment of Fe and K metals at locations
471 exposed to PHB. It must be kept in mind that PM_{10} samples included coarse mode aerosols, of which dust might have been a
472 significant fraction. Also, environmental regulations have been successful in steadily reducing the sugarcane burned area in
473 the CRV since 2009. The burned area dropped from 72% in 2011 to 35.46% in 2018, our year of measurements (Cardozo-
474 Valencia et al., 2019).

475

476 Cd, Pb, Ni, Hg and As, and other metals and metalloids are considered carcinogenic (WHO Regional Office for Europe, 2020).
477 Measured concentrations of Pb and Ni in $PM_{2.5}$ at CRV were 18 ng m^{-3} (+/-19) and 2 ng m^{-3} (+/-1), respectively. These mean
478 values were below the EU target values of ($0.5 \mu\text{g m}^{-3}$ and 20 ng m^{-3} respectively) (WHO, 2013a), and below the annual
479 average limit of the Colombian national ambient air quality standard ($0.5 \mu\text{g m}^{-3}$ and $0.18 \mu\text{g m}^{-3}$ respectively) (MADS, 2017).
480 Nevertheless, these concentrations are significantly higher than those reported for other suburban areas in Midwestern United
481 States and remote sites in the northern tropical Atlantic (Fomba et al., 2018; Kundu and Stone, 2014). Pb concentrations are

482 similar to those reported for Bogotá and other large urban areas (SDA, 2010; Vasconcellos et al., 2007). Pb has been long
483 banned as a fuel additive in Colombia, thus the observed levels might be associated with metallurgical industry and waste
484 incineration. Information on ambient air hazardous metal concentrations in Latin America's urban and rural areas is still scarce.
485

486 **3.5. Carbohydrates**

487
488 Levoglucosan is a highly specific biomass burning organic tracer (Bhattarai et al., 2019). Along with K^+ , OC and EC, it can
489 be used to effectively identify the relevance of biomass burning as an aerosol source. The relative contribution of levoglucosan
490 to the PM carbohydrate burden, and especially the levoglucosan to mannosan ratio, can be used as indicators of the type of
491 biomass burned (Engling et al., 2009). In this study, the following carbohydrates were quantified: levoglucosan, mannosan,
492 glucose, galactosan, fructose and arabitol. Levoglucosan was by far the most abundant ($113.8 \pm 147.2 \text{ ng m}^{-3}$), reaching values
493 of up to 904.3 ng m^{-3} , followed by glucose ($10.4 \pm 6.1 \text{ ng m}^{-3}$), mannosan ($7 \pm 6.1 \text{ ng m}^{-3}$), and arabitol ($4.1 \pm 3.5 \text{ ng m}^{-3}$).
494 Levoglucosan and mannosan were detected in all $PM_{2.5}$ samples, while galactosan and fructose were detected only in 9 and 11
495 samples, respectively. Levoglucosan was $3.5 \pm 2.3\%$ of OC and $0.96\% \pm 0.81\%$ of $PM_{2.5}$.

496
497 The levoglucosan concentration found in this study was quite similar to that reported in areas of Brazil where sugarcane
498 production and processing are important economic activities, Figure 3. For instance, during the harvest (*zafra*) period in
499 Araraquara, the levoglucosan mean concentration was $138 \pm 91 \text{ ng m}^{-3}$, although during the non-harvest period it was
500 unexpectedly high ($73 \pm 37 \text{ ng m}^{-3}$) (Urban et al., 2014). Likewise, the levoglucosan average concentration at Piracicaba during
501 a reduced fire period was 66 ng m^{-3} (Souza et al., 2014). The measured mean levoglucosan/mannosan ratio in CRV was 17.6
502 ± 13.0 (min: 8.1 – max: 58.1). Chemical profile studies found a levoglucosan/mannosan ratio of ~ 10 for sugarcane leaves
503 burned in stoves (Hall et al., 2012; Dos Santos et al., 2002) and of ~ 54 for burned bagasse (Dos Santos et al., 2002). Leaves
504 constitute the largest fraction (20.8%, Victoria et al., 2002) of pre-harvest burned sugarcane. Consistently and expectably, the
505 levoglucosan/mannosan ratio in this study was much closer to the chemical profile ratio of leaves than that of bagasse.
506 Moreover, ambient air samples in Araraquara and Piracicaba showed levoglucosan/mannosan ratios of 9 ± 5 and ~ 33 ,
507 respectively. For comparison, the levoglucosan/mannosan ratio in PM from rice straw and other crops burned were ~ 26.6
508 and ~ 23.8 , respectively (Engling et al., 2009). This indicates that the levoglucosan/mannosan ratio is sensitive to the type of
509 biomass burned but also to burning conditions. The large levoglucosan/mannosan ratio in our study suggests that in CRV was
510 impacted by sugarcane PHB most of the time, and, to a lesser extent, by bagasse combustion in sugar mills. We hypothesize
511 that, even if these were very small, levoglucosan and mannosan combustion emissions might not be negligible as the CRV
512 sugarcane biomass yields are very high and most of the harvested sugarcane bagasse is combusted for electric power and steam
513 production.

514

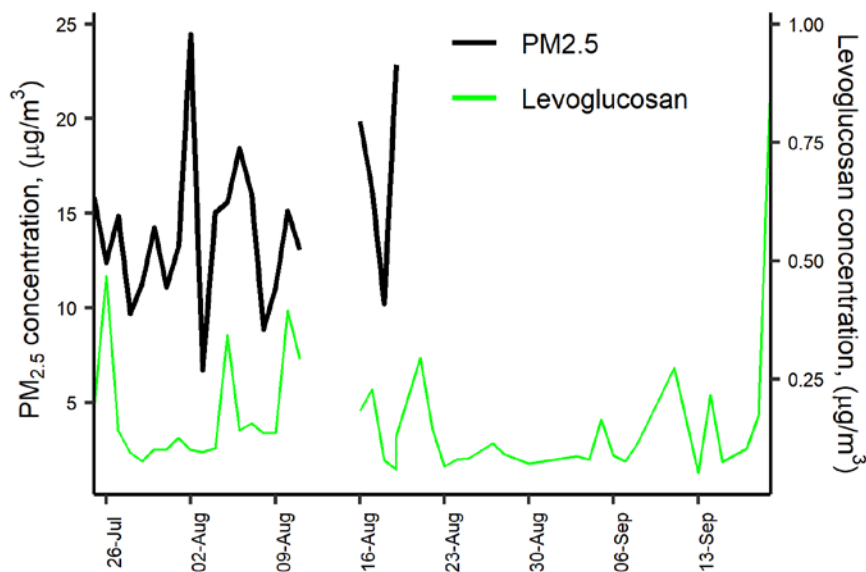


Figure 3. Daily variation of Levoglucosan and PM_{2.5} concentration at CRV.

515

516

517 3.6. Polycyclic Aromatic Hydrocarbons (PAHs)

518

519 A total of 22 PAHs were measured in each sample collected at Palmira, including the 16 PAHs listed as human health priority
 520 pollutants by WHO and US-EPA (Yan et al., 2004). The total PAHs concentration was $5.6 \pm 2.9 \text{ ng m}^{-3}$ (min: 2.3 ng m^{-3} –
 521 max: 15.8 ng m^{-3}). Figure 4a shows the PAHs concentration variability during the sampling campaign (mean and standard
 522 deviation are available in Table S2). The most abundant PAH were FLE ($44.2\% \pm 11.9\%$ total concentration share), ANT (9,10)
 523 ($10.0\% \pm 4.5\%$), BbF ($7.4\% \pm 2.3\%$), BghiP ($6.7\% \pm 2.4\%$), IcdP ($6.4\% \pm 1.9\%$), CPY ($6.0\% \pm 2.3\%$), FLO (9H) ($5.4\% \pm 3.1\%$),
 524 BeP ($4.6\% \pm 1.3\%$), and BaP ($4.4\% \pm 1.6\%$), which accounted for 95.1% of the total PAH concentration (Figure 4b). Three-ring
 525 PAHs were the most abundant (59.04% of total PAH). Put together, five- and six-ring PAHs accounted for an additional
 526 38.44%. The less abundant PAH group was the four-ring (2.52%). A previous study in CRV, carried out on PM₁₀ samples by
 527 Romero et al. (2013), showed higher FLT, PYR, and PHE concentrations in areas highly exposed to sugarcane PHB compared
 528 to other locations. In contrast, PM_{2.5} FLE concentrations in this research were significantly higher than those in PM₁₀ by
 529 Romero et al. (2013), while PYR and PHE levels were similar.

530

531 The carcinogenic species BaP, BbF, BkF, BaA, BghiP, FLE, CPY and BeP were identified in all the PM_{2.5} samples. BaP is a
 532 reference for PAH carcinogenicity (WHO, 2013a) that is used as a PAH exposure metric, known as the Benzo(a)Pyrene-
 533 equivalent carcinogenic potency (BaPE). We calculated BaPE using the toxic equivalent factors (TEF) proposed by Nisbet

534 and LaGoy (1992) and (Malcolm and Dobson, 1994). PAH concentrations were multiplied by TEF and then added to estimate
535 the carcinogenic potential of PM_{2.5}-bounded PAHs. The mean carcinogenicity level at Palmira, expressed as BaP-TEQ, was
536 $0.4 \pm 0.2 \text{ ng m}^{-3}$ (min: 0.1 ng m^{-3} - max: 1.4 ng m^{-3}). Only one sample exceeded the Colombian annual limit of 1 ng m^{-3} but
537 most of them exceeded the WHO reference level of 0.12 ng m^{-3} . The mutagenic potential of PAHs (BaP-MEQ) was estimated
538 using the mutagenic equivalent factors (MEF) reported by Durant et al., (1996). The average BaP-MEQ was $0.5 \pm 0.3 \text{ ng m}^{-3}$
539 (min: 0.2 ng m^{-3} - max: 1.8 ng m^{-3}). These levels are comparable to those measured in PM_{2.5} by Mugica-Álvarez et al., (2016)
540 in Veracruz (Mexico) but during the sugarcane non-harvest period. PM₁₀ BaP-MEQ levels in Araraquara (Brazil) (de Andrade
541 et al., 2010; De Assuncao et al., 2014) were twice as high as those found in this study. This suggests that year-long sugarcane
542 PHB in the CRV leads to lower mutagenic potentials compared to those at locations where the harvesting period (*zafra*) is
543 shorter, thus with higher burning rates. We estimated the average BaP-TEQ and BaP-MEQ concentrations in the CRV
544 according to their exposure to sugarcane burning products from Romero et al., (2013) data and used them as a benchmark to
545 our measurements. PM₁₀-bound BaP-TEQ and BaP-MEQ levels for areas not directly exposed to sugarcane burning were 0.16
546 ng m^{-3} and 0.21 ng m^{-3} , respectively. Toxicity and mutagenicity due to PM₁₀-bound PAHs were 4 times as high as those at
547 areas directly exposed to sugarcane burning. It is reasonable to assume that PAHs are largely bound to fine aerosol ($<2.5 \mu\text{m}$),
548 thus that our measurements are comparable to (Romero et al., 2013). If so, our site of observation would be at an intermediate
549 exposure condition, higher than areas not directly exposed to sugarcane burning but lower than directly exposed areas.

550

551 Ratios among different PAHs have been extensively used to distinguish between traffic and other PAH sources. We used the
552 diagnostic ratios presented by Ravindra et al. (2008) and Tobiszewski and Namieśnik (2012a) to better understand the
553 contribution of sources to PM_{2.5} in the CRV. The ratio benzo(e)pyrene to the sum of benzo(e)pyrene and benzo(a) pyrene is
554 used as an indicator of aerosol aging. Local or “fresh” aerosols have $[\text{BeP}]/([\text{BeP}]+[\text{BaP}])$ ratios around 0.5, while aged
555 aerosols can have ratios as low as zero as a result of photochemical decomposition and oxidation. The $[\text{BeP}]/([\text{BeP}]+[\text{BaP}])$
556 ratio at Palmira was 0.51 ± 0.04 , with a majority (84.4%, $n = 38$) of fresh samples a minor fraction (15.6%, $n=7$) of
557 photochemically-degraded samples.

558

559 Other two diagnostic ratios were used to assess the prevalence of traffic as a PM_{2.5} source. The first ratio used IcdP BghiP, two
560 automobile emissions markers (Miguel and Pereira, 1989). Values higher than 0.5 for the ratio $[\text{IcdP}]/([\text{IcdP}]+[\text{BghiP}])$
561 indicates aged particles (Tobiszewski and Namieśnik, 2012) generated by coal, grass or wood burning (Yunker et al., 2002).
562 The second ratio is $[\text{BaP}]/[\text{BghiP}]$. Ratios higher than 0.6 are indicative of traffic emissions (Tobiszewski and Namieśnik,
563 2012). At Palmira, the $[\text{IcdP}]/([\text{IcdP}]+[\text{BghiP}])$ and $[\text{BaP}]/[\text{BghiP}]$ ratios were 0.48 ± 0.04 and 0.69 ± 0.13 , which indicates
564 that ~63% of the samples originated from combustion of oil products ($n = 30$), and ~36% came from non-traffic sources, like
565 wood, grass, or coal ($n = 15$).

566

567 Also, the structure and size of PAHs are indicative of their sources. PAHs of low molecular weight (LMW) (two or three
568 aromatic rings) have been reported as tracers of wood, grass, and fuel oil combustion, while those of medium molecular weight
569 (MMW) (four rings) and high molecular weight (HMW) (five and six rings) are associated with coal combustion and vehicular
570 emissions. The ratio between LMW and the sum of MMW and HMW, $LMW/(MMW+HMW)$, is used for source identification.
571 Ratios lower than one are indicative of oil products combustion, while ratios larger than one are associated with coal and
572 biomass combustion (Tobiszewski and Namieśnik, 2012). The ratio at Palmira, $LMW/(MMW+HMW) = 1.43 \pm 1.00$, was
573 rather variable but suggests that a large fraction of PAHs in CRV (82.2% of samples) were generated by biomass burning or
574 combustion, as well as coal combustion in brick kilns. Just one in five samples (17.8%) had PAHs attributable to oil product
575 combustion.

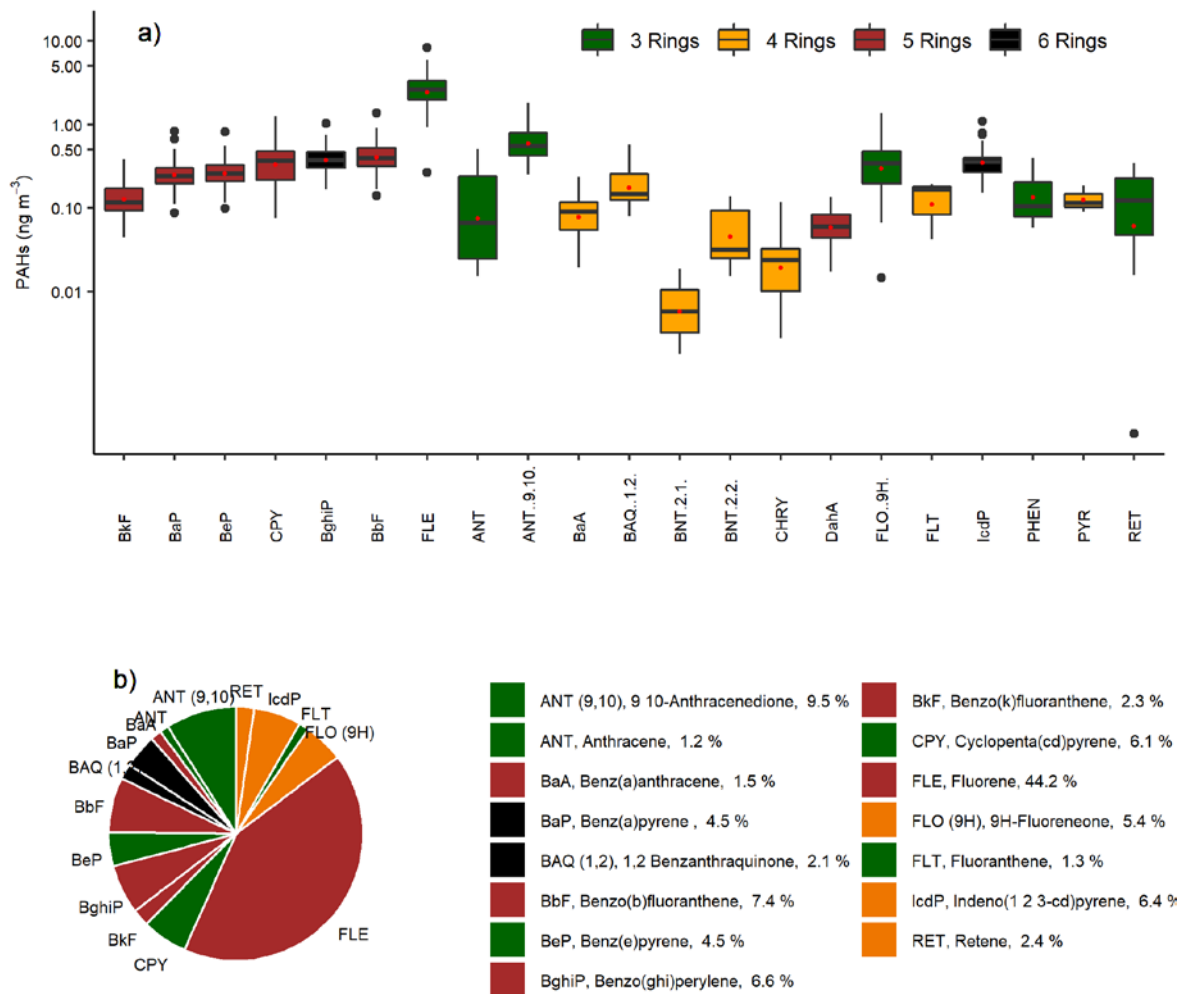
576

577 Sugarcane-burning emitted PAH are mainly LMW, especially of two (~66% of PAHs) and three rings (~27%), among which
578 FLE, PHE and ANT are the most emitted, according to Hall et al. (2012) chemical profile. The relative abundance of 3-ring
579 PAHs (Figure 4) in CRV's $PM_{2.5}$ is likely due to open-field sugarcane PHB to a major extent, and to controlled bagasse
580 combustion for electric power and steam production, to a lesser extent.

581

582 The highest PAH concentrations were observed on 10th August and 11th September 2018, with levels of 15.8 ng m^{-3} and 14.4
583 ng m^{-3} , respectively (Fig 5S). Elevated concentrations of 5 and 6 ring PAHs were observed on 10th August 2018. A change in
584 the wind circulation pattern was observed on the previous day (Fig S2), with a wind speed reduction and a predominance of
585 winds from the north. Later, on 11th September 2018, we observed an increase in 3-ring PAHs and winds from the NW at the
586 average wind speed at the sampling location. This indicates that there were at least two types of sources. The abundance of
587 HMW PAHs indicates fossil fuel combustion sources, and LMW PAHs suggest that parts of these come from non-fossil fuel
588 combustion sources.

589



590

591 Figure 4. The abundance of PAHs measured in PM_{2.5} samples collected in CRV, represented by colors according to the number
 592 of rings of each PAH, green (tree rings), yellow (four rings), brown (five rings), and black (six rings). a) Boxplot of
 593 concentrations in ng m⁻³, red dots represent mean concentrations of each PAH. b) pie-plot of the relative abundance of PAHs
 594 in PM_{2.5} samples.

595 3.7. Alkanes

596

597 A total of 16 alkanes ranging from C₂₀ up to C₃₄ were analyzed in this study and used to identify the presence of fossil fuel
 598 combustion and plant fragments in the PM_{2.5} samples. The abundance of total n-alkanes during the whole sampling period was
 599 in the range of 13.0 to 88.45 ng m⁻³ with an average concentration of 40.36 ng m⁻³ ± 18.82 ng m⁻³. In general, the high molecular
 600 weight n-alkanes such as C₂₉ – C₃₁ were the most abundant. These are characteristic of vegetative detritus corresponding to
 601 plant fragments in airborne PM (Lin et al., 2010). The most abundant n-alkanes were C₂₉, C₃₀, and C₃₁ (Fig 6.). Likewise, the

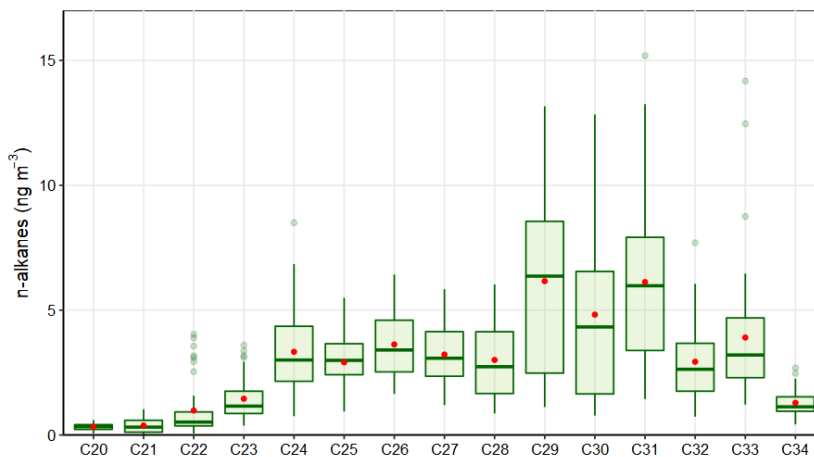
602 carbon number maximum concentration (C_{\max}) was C_{29} in 43% of samples and C_{31} in 28% of them. This result is consistent
603 with the chemical profile of sugarcane burning reported by (Oros et al., 2006) with a C_{\max} of C_{31} .
604

605 The carbon preference index (CPI) and wax n-alkanes percentage (WNA%) are parameters used to elucidate the origin of the
606 n-alkanes and infer whether emissions come from biogenic or anthropogenic sources. The CPI represents the ratio between
607 odd and even carbon number n-alkanes. The equation used to calculate CPI in the present study is shown in Table 2, following
608 the procedure reported by (Marzi et al., 1993). Values of $CPI \leq 1$ (or close to 1) indicate that n-alkanes are emitted from
609 anthropogenic sources, while values higher than 1 indicate the influence of vegetative detritus and biomass burning in the
610 $PM_{2.5}$ samples (Mancilla et al., 2016). In this study, the mean CPI was always greater than 1, with an average value of $1.22 \pm$
611 0.18 (min:1.02 – max:1.8) that is between the CPI for fossil fuel emissions of ~ 1.0 (Caumo et al., 2020) and sugarcane burning
612 of 2.1 (Oros et al., 2006), revealing the influence of several sources over the $PM_{2.5}$ in the CRV.
613

614 Likewise, WNA% represents the preference of odd n-alkanes in the sample. The odd n-alkanes, especially of higher molecular
615 weight, are representative of plant wax related emissions. The waxes are present on the surface of plants, especially on the
616 leaves, and they become airborne by a direct or indirect mechanism like wind action or biomass burning (Kang et al., 2018;
617 Simoneit, 2002). In this research, the samples analyzed showed a preference for odd carbon on C_{27} , C_{29} , C_{31} and C_{33} , which
618 have higher concentrations than the next higher and lower even carbon number homologs, proving the biogenic contribution
619 over the $PM_{2.5}$ in the CRV. The WNA% was calculated using the equation shown in Table 2, described by Yadav et al. (2013).
620 A larger WNA% represents the contribution from emissions of plant waxes or biomass burning. Otherwise, a smaller value
621 represents n-alkanes from petrogenic sources, known as petrogenic n-alkanes (PNA)%. The mean WNA% calculated for the
622 $PM_{2.5}$ samples collected from the CRV was $12.65\% \pm 5.21\%$ (min: 4.71% – max: 29.92%) and can be defined as petrogenic
623 inputs (PNA%) that were 87.35% during the sampling period. The correlation between CPI and WNA was moderate ($r^2=0.53$)
624 supporting a consistent meaning between these two parameters, and they are useful for assessing the plant wax contribution to
625 $PM_{2.5}$.
626

627 Overall, the total concentration of n-alkanes in the $PM_{2.5}$ in the CRV was lower than those reported in areas where sugarcane
628 is often burned in Brazil (Urban et al., 2016), although the behavior of the parameters of CPI and C_{\max} is similar. Compared
629 with other urban areas in Latin America, the n-alkane concentration in the CRV was similar to that reported in the metropolitan
630 zone of the Mexican valley (MZMV) for $PM_{2.5}$ (Amador-Muñoz et al., 2011), Bogotá for PM_{10} and slightly lower than reported
631 in Sao Paulo for PM_{10} (Vasconcellos et al., 2011). However, the CPI and WNA in these cities were smaller than in the CRV,
632 because of the strong influence of vehicular emissions in these densely populated cities. The OC/EC ratio was moderately
633 associated with WNA values ($r^2 = 0.41$), indicating that an increase in this ratio can be explained by the vegetative detritus
634 contribution to $PM_{2.5}$, while the levoglucosan concentrations did not show correspondence to the CPI and WNA values;
635 therefore, the levoglucosan levels did not explain the preference of odd carbon number homologs. These results indicated that

636 the n-alkanes found in this study came from several sources, with a noticeable contribution from plant wax emissions. The
637 parameters used to assess the source contribution of PM_{2.5} through n-alkanes such as CPI and WNA%, were characteristic of
638 aerosols collected in urban areas.
639



640
641 Figure 5. Average n-alkanes concentrations in PM_{2.5} samples

642 3.8. PM_{2.5} mass closure

643

644 Mass closure (Figure 6) shows the crucial contribution of organic material ($52.66 \pm 18.44\%$) and inorganic fraction, represented
645 by sulfate ($12.69 \pm 2.84\%$), ammonium ($3.75 \pm 1.05\%$), nitrate ($2.56 \pm 1.29\%$). EC constituted $7.13 \pm 2.44\%$ of PM_{2.5}. The
646 mineral fraction corresponded to dust ($3.51 \pm 1.35\%$) and TEO ($0.85 \pm 0.42\%$). Mass closure of $88.42 \pm 24.17\%$ was achieved.
647 Although PM_{2.5} concentrations observed in the CRV were not so high as compared with those registered in Brazil and Mexico
648 during the preharvest season, the EC percentage is in a similar range or slightly lower than those observed in other urban areas
649 (Snider et al., 2016), showing the key role of incomplete combustion processes in the area.

650

651 The average (OC/EC) ratio found in CRV was 4.2 ± 0.72 , from which we can infer that secondary aerosol formation had a
652 relevant role. The segregation of OC into the primary and secondary fractions was carried out using two methods. The first
653 was the EC tracer method applied in previous studies (Pio et al., 2011; Plaza et al., 2011), and the second was the organic
654 tracer method, which is based on the lineal regression between OC and organic tracers from primary sources. In the EC tracer
655 method, the (OC/EC)_{min} ratio selected to differentiate OC_{prim} from OC_{sec} was the minimum ratio observed, equivalent to 2.12.
656 Still, this value could induce the overestimation of OC_{prim} due to the distance between the emission sources and the sampling
657 site (27 m aboveground), and the local meteorological conditions that favor the volatilization and oxidation of organic
658 components into particles before being collected. As a result, OC_{prim} was estimated at 50.3% and OC_{sec} at 49.7% of the total

659 OC, with a minimum variability of 3.8%. The estimated OM_{pri} concentration was $3.22 \pm 1.09 \mu\text{g m}^{-3}$ and the OM_{sec}
660 concentration was $4.01 \pm 1.78 \mu\text{g m}^{-3}$, which represented 24.2% and 28.5% of $PM_{2.5}$ respectively.

661

662 In the organic tracer method, the contribution of fossil fuel combustion - mainly derived from transport -, biomass burning,
663 and vegetative detritus to OC_{prim} was estimated from a linear model by robust regression using an M estimator with bisquare
664 function between organic tracers and OC. Resulting contributions were as follows: OC_{ff} : 16.38%, OC_{bb} : 15.19%, and OC_{det} :
665 1.45% of total OC measured. Overall, the use organic tracer method to estimate OC_{prim} indicates that this carbonaceous fraction
666 represents $32.68\% \pm 11.02\%$ of total OC, and it may fluctuate between 17.61% and 68.60%.

667

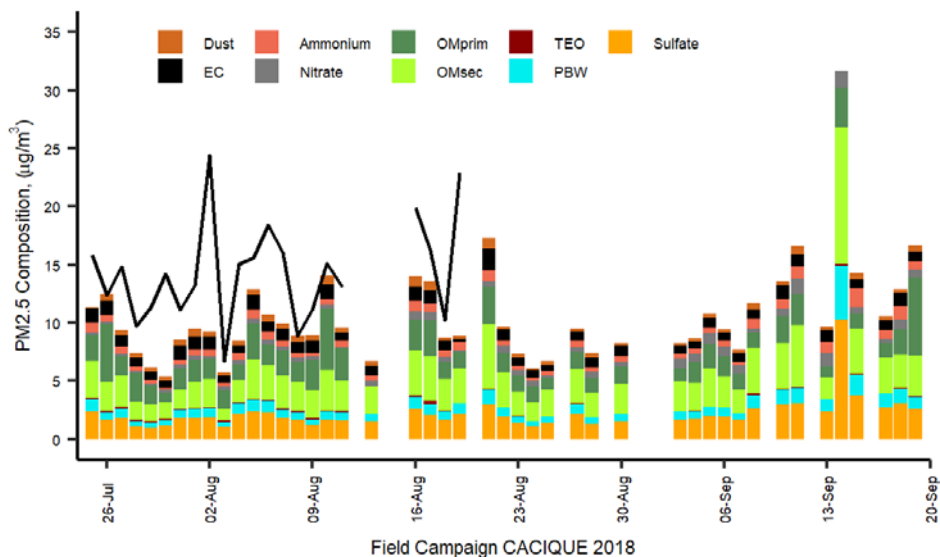
668 The difference between OC_{prim} from the organic tracer method and that obtained from the EC tracer method can be associated
669 to the fact that the organic tracer method may not be representative of all sources. Industrial coal and fuel oil burning, garbage
670 burning, cooking, charcoal production and other sources may not be accounted for by this method, since we did not have
671 specific organic tracers for each of these activities.

672

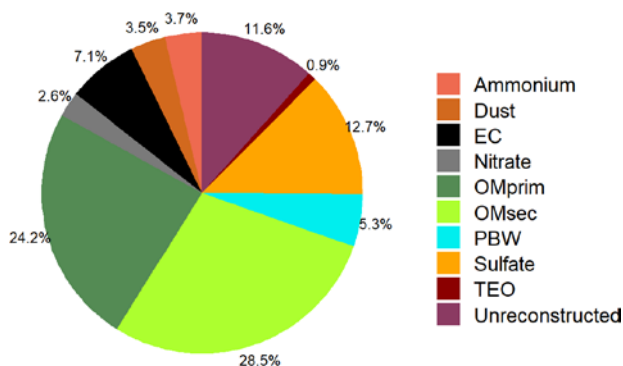
673 The mineral fraction, quantified as the sum of the oxides present in the crustal material (dust) and other TEO contributed $3.51 \pm$
674 1.35% and $0.85 \pm 0.42\%$, respectively. Despite the non-quantification of highly abundant mineral dust elements such as Si,
675 the concentrations of Ca, Ti, and Fe indicated the impact of soil resuspension on the $PM_{2.5}$ mass concentration.

676

677 PBW depends on the concentration of hygroscopic compounds embodied in the PM and the relative humidity of the weighing
678 room where $PM_{2.5}$ mass collected on the filters was determined. In this study, it was assumed that (i) NH_4^+ , SO_4^{2-} and NO_3^-
679 were the main compounds responsible for absorbed water and (ii) thermodynamic equilibrium is dominated by these ions that
680 allow calculating the H^+ molar fraction as a difference between $(SO_4^{2-} + NO_3^-)$ and NH_4^+ , which is required to establish charge
681 neutrality. Polar organic compounds and other water-soluble ions were not considered in the present study. The PBW content
682 was estimated using the mean measured concentrations of NH_4^+ , SO_4^{2-} and NO_3^- in the AIM Model, where a multiplier factor
683 of 0.32 was found as a proportion between the concentrations of the sum of these ions and the water fraction contained in
684 $PM_{2.5}$. As a result, PBW was 5.3% of the $PM_{2.5}$ mass concentration.



685



686

687 Figure 6. Mass reconstruction of PM_{2.5} collected in CRV. Figure in upper corresponding to timeseries of PM_{2.5} gravimetric
 688 mass measured and reconstructed mass from the chemical speciation in CRV during July – September 2018 and lower is the
 689 to pie plot the relative mean contributions (%) of major chemical components of gravimetric PM_{2.5} based on chemical
 690 speciation.

691

692 **4. Conclusions**

693 PM_{2.5} samples collected in the Cauca River Valley, Colombia, were analyzed to determine the main chemical components of
 694 fine aerosol particles and to qualitatively identify aerosol sources using its chemical composition and diagnostic ratios. PM_{2.5}

695 during the campaign was $14.4 \pm 4.4 \mu\text{g m}^{-3}$. Its main components were OC ($4.0 \pm 1.3 \mu\text{g m}^{-3}$), sulfate ($2.2 \pm 1.4 \mu\text{g m}^{-3}$), and
696 EC ($1.0 \pm 0.3 \mu\text{g m}^{-3}$), ammonium ($0.7 \pm 0.6 \mu\text{g m}^{-3}$), and nitrate ($0.5 \pm 0.3 \mu\text{g m}^{-3}$). OM was estimated using the EC tracer
697 method and the organic tracer method. Mass closure using the EC tracer method explained 88.4% of $\text{PM}_{2.5}$, whereas the organic
698 tracer method explained 70.9% of $\text{PM}_{2.5}$. We attribute this difference to the lack of information of specific organic tracers for
699 some sources, both primary and secondary. Organic material and inorganic ions were the dominant groups of species,
700 constituting almost 79% of $\text{PM}_{2.5}$. OM_{prim} and OM_{sec} from the EC tracer method contribute 24.2% and 28.5% to $\text{PM}_{2.5}$.
701 Inorganic ions made up 19.0%, EC 7.1%, dust 3.5%, PBW 5.3%, and TEO 0.9% of $\text{PM}_{2.5}$.

702

703 Aerosol acidity was evaluated using three methods. The first, using the nitrate/sulfate ratio; the second using the anion/cation
704 equivalent ratio; and the third, estimating the pH with the E-AIM thermodynamic model. All methods showed that the aerosol
705 was acidic, with a pH of 2.5 ± 0.4 , mainly because of the abundance of organic and sulfur compounds.

706

707 Diagnostic ratios applied to organic compounds indicate that most $\text{PM}_{2.5}$ was emitted locally and had contributions of both
708 pyrogenic and petrogenic sources. In addition, levoglucosan and mannosan levels showed that biomass burning was ubiquitous
709 during the sampling period. Fluoranthene (FLE) was the most abundant PAH, confirming the strong influence of BB associated
710 with agro-industry. Five- and six-ring PAH associated with vehicular emissions were also abundant in $\text{PM}_{2.5}$. Our
711 measurements point to BB as the main source of PAHs in CRV. Relatively low $\text{PM}_{2.5}$ concentrations and mutagenic potentials
712 are consistent with low-intensity, year-long BB and sugarcane PHB in CRV, which leads to lower atmospheric pollutant
713 burdens and mutagenic potentials compared to those at locations where the harvesting period is shorter (*zafra*) thus with higher
714 burning rates.

715 *Author contribution:* RJ, GR-S, and NR conceived and managed the project. LM-F, ACV-B, GR-S, and RJ set the instruments
716 up and performed the aerosol sampling. LM-F carried out the sample chemical analysis at TROPOS with the guidance and
717 support of DvP, MvP, KW, and HH. LM-F and ACV-B analyzed the measurement results, including PCA and other techniques
718 with the support of DvP and LM-F, RJ, NR and ACV-B prepared the manuscript with substantial contributions from all the
719 authors.

720 *Competing interests:* The authors declare that they have no conflict of interest.

721 *Acknowledgments:* The authors gratefully acknowledge the financial support from Universidad Nacional de Colombia – Sede
722 Palmira (Project “Impacto de la quema de caña de azúcar en la calidad del aire del Valle Geografico del Río Cauca
723 (CACIQUE), Hermes # 37718), and Leibniz Institute for Tropospheric Research (TROPOS) for analytical support. This project
724 was supported by EU granted the mobility project PAPILA. We thank Susanne Fuchs, Anke Roedger, Sylvia Haferkorn, and

725 Kornelia Pielok for their technical assistance in the chemical analysis of samples. We acknowledge Pablo Gutierrez for his
726 contributions in the processing of the open sugarcane burning database and for preparing the CRV map.

727 **References**

728 Aerocivil: Estadísticas Operacionales, Operaciones aéreas Total. 2000-2019
729 <https://www.aerocivil.gov.co/atencion/estadisticas-de-las-actividades-aeronauticas/estadisticas-operacionales>, last access: 15
730 February 2022, 2019.

731 Agarwal, A., Satsangi, A., Lakhani, A. and Kumari, K. M.: Seasonal and spatial variability of secondary inorganic aerosols in
732 PM_{2.5} at Agra: Source apportionment through receptor models, *Chemosphere*, 242, 125132,
733 <https://doi.org/10.1016/j.chemosphere.2019.125132>, 2020.

734 Alvi, M. U., Kistler, M., Shahid, I., Alam, K., Chishtie, F., Mahmud, T. and Kasper-Giebl, A.: Composition and source
735 apportionment of saccharides in aerosol particles from an agro-industrial zone in the Indo-Gangetic Plain, *Environ. Sci. Pollut.*
736 *Res.* 2020 2712, 27(12), 14124–14137, <https://doi.org/10.1007/S11356-020-07905-2>, 2020.

737 Amador-Muñoz, O., Villalobos-Pietrini, R., Miranda, J. and Vera-Avila, L. E.: Organic compounds of PM_{2.5} in Mexico
738 Valley: Spatial and temporal patterns, behavior and sources, *Sci. Total Environ.*, 409(8), 1453–1465,
739 <https://doi.org/10.1016/j.scitotenv.2010.11.026>, 2011.

740 de Andrade, S. J., Cristale, J., Silva, F. S., Julião Zocolo, G. and Marchi, M. R. R.: Contribution of sugar-cane harvesting
741 season to atmospheric contamination by polycyclic aromatic hydrocarbons (PAHs) in Araraquara city, Southeast Brazil,
742 *Atmos. Environ.*, 44(24), 2913–2919, <https://doi.org/10.1016/j.atmosenv.2010.04.026>, 2010.

743 Andreae, M. O.: Soot Carbon and Excess Fine Potassium : Long-Range Transport of Combustion-Derived Aerosols., 1983.

744 Aneja, V. P., Schlesinger, W. H. and Erisman, J. W.: Farming pollution, *Nat. Geosci.*, 1(7), 409–411,
745 <https://doi.org/10.1038/ngeo236>, 2008.

746 Aneja, V. P., Schlesinger, W. H. and Erisman, J. W.: Effects of agriculture upon the air quality and climate: Research, policy,
747 and regulations, *Environ. Sci. Technol.*, 43(12), 4234–4240, <https://doi.org/10.1021/es8024403>, 2009.

748 Asocaña: Aspectos Generales del Sector Agroindustrial de la Caña 2017 - 2018. Informe Anual. <https://www.asocana.org>,
749 2018.

750 Asocaña: Aspectos generales del sector agroindustrial de la caña Informe anual 2018-2019.
751 [https://www.asocana.org/documentos/2352019-D0CA1EED-](https://www.asocana.org/documentos/2352019-D0CA1EED-00FF00,000A000,878787,C3C3C3,0F0F0F,B4B4B4,FF00FF,2D2D2D,A3C4B5.pdf)

752 [00FF00,000A000,878787,C3C3C3,0F0F0F,B4B4B4,FF00FF,2D2D2D,A3C4B5.pdf](https://www.asocana.org/documentos/2352019-D0CA1EED-00FF00,000A000,878787,C3C3C3,0F0F0F,B4B4B4,FF00FF,2D2D2D,A3C4B5.pdf), last access: 20 May 2020, 2019.

753 De Assuncao, J. V., Pesquero, C. R., Nardocci, A. C., Francisco, A. P., Soares, N. S. and Ribeiro, H.: Airborne polycyclic
754 aromatic hydrocarbons in a medium-sized city affected by preharvest sugarcane burning and inhalation risk for human health,
755 *J. Air Waste Manag. Assoc.*, 64(10), 1130–1139, <https://doi.org/10.1080/10962247.2014.928242>, 2014.

756 Begam, G. R., Vachaspati, C. V., Ahammed, Y. N., Kumar, K. R., Reddy, R. R., Sharma, S. K., Saxena, M. and Mandal, T.

757 K.: Seasonal characteristics of water-soluble inorganic ions and carbonaceous aerosols in total suspended particulate matter at
758 a rural semi-arid site, Kadapa (India), *Environ. Sci. Pollut. Res.*, 24(2), 1719–1734, [https://doi.org/10.1007/s11356-016-7917-](https://doi.org/10.1007/s11356-016-7917-1)
759 1, 2016.

760 Bhattarai, H., Saikawa, E., Wan, X., Zhu, H., Ram, K., Gao, S., Kang, S., Zhang, Q., Zhang, Y., Wu, G., Wang, X., Kawamura,
761 K., Fu, P. and Cong, Z.: Levoglucosan as a tracer of biomass burning: Recent progress and perspectives, *Atmos. Res.*,
762 220(November 2018), 20–33, <https://doi.org/10.1016/j.atmosres.2019.01.004>, 2019.

763 Boman, J., Lindén, J., Thorsson, S., Holmer, B. and Eliasson, I.: A tentative study of urban and suburban fine particles (PM_{2.5})
764 collected in Ouagadougou, Burkina Faso, *X-Ray Spectrom.*, 38(4), 354–362, <https://doi.org/10.1002/XRS.1173>, 2009.

765 Cardozo-Valencia, A., Saa, G. R., Hernandez, A. J., Lopez, G. R. and Jimenez, R.: Distribución espaciotemporal y estimación
766 de emisiones por quema precosecha de caña de azúcar en el Valle del Cauca, *Conf. Proc. - Congr. Colomb. y Conf. Int. Calid.*
767 *Aire y Salud Publica, CASAP 2019*, <https://doi.org/10.1109/CASAP.2019.8916696>, 2019.

768 Casey, K. D., Bicudo, J. R., Schmidt, D. R., Singh, A., Gay, S. W., Gates, R. S., Jacobson, L. D. and Hoff, S. J.: Air quality
769 and emissions from livestock and poultry production / waste management systems, in *Animal Agriculture and the*
770 *Environment*, National Center for Manure & Animal Waste Management White Papers, pp. 1–40, , 2006.

771 Caumo, S., Bruns, R. E. and Vasconcellos, P. C.: Variation of the distribution of atmospheric n-alkanes emitted by different
772 fuels' combustion, *Atmosphere (Basel)*, 11(6), 1–19, <https://doi.org/10.3390/atmos11060643>, 2020.

773 Cavalli, F., Viana, M., Yttri, K. E., Genberg, J. and Putaud, J.: Toward a standardised thermal-optical protocol for measuring
774 atmospheric organic and elemental carbon: the EUSAAR protocol, *Atmos. Meas. Tech.*, 3, 79–89,
775 <https://doi.org/10.5194/amt-3-79-2010>, 2010.

776 Chow, J. C., Lowenthal, D. H., Chen, L. W. A., Wang, X. and Watson, J. G.: Mass reconstruction methods for PM_{2.5}: a
777 review, *Air Qual. Atmos. Heal.*, 8(3), 243–263, <https://doi.org/10.1007/s11869-015-0338-3>, 2015.

778 Clegg, S. L., Brimblecombe, P. and Wexler, A. S.: Thermodynamic Model of the System H⁺–NH₄⁺–SO₄²⁻–NO₃–H₂O at
779 Tropospheric Temperatures, *J. Phys. Chem. A*, 102(12), 2137–2154, <https://doi.org/10.1021/jp973042r>, 1998.

780 Criollo, J. and Daza, N.: Evaluación de los niveles de concentración de metales en PM 10 producto de la quema de biomasa
781 en el valle geográfico del rio Cauca, La Salle University https://ciencia.lasalle.edu.co/ing_ambiental_sanitaria/135%0AThis,
782 2011.

783 Dabek-Zlotorzynska, E., Dann, T. F., Kalyani Martinelango, P., Celso, V., Brook, J. R., Mathieu, D., Ding, L. and Austin, C.
784 C.: Canadian National Air Pollution Surveillance (NAPS) PM_{2.5} speciation program: Methodology and PM_{2.5} chemical
785 composition for the years 2003-2008, *Atmos. Environ.*, 45(3), 673–686, <https://doi.org/10.1016/j.atmosenv.2010.10.024>,
786 2011.

787 Durant, J. L., Busby Jr, W. F., Lafleur, A. L., Penman, B. W. and Crespi, C. L.: Human cell mutagenicity of oxygenated,
788 nitrated and unsubstituted polycyclic aromatic hydrocarbons associated with urban aerosols, *Mutat. Res. - Genet. Toxicol.*,
789 371(3–4), 123–157, [https://doi.org/10.1016/S0165-1218\(96\)90103-2](https://doi.org/10.1016/S0165-1218(96)90103-2), 1996.

790 El-Zanan, H. S., Lowenthal, D. H., Zielinska, B., Chow, J. C. and Kumar, N.: Determination of the organic aerosol mass to

791 organic carbon ratio in IMPROVE samples, *Chemosphere*, 60(4), 485–496,
792 <https://doi.org/10.1016/j.chemosphere.2005.01.005>, 2005.

793 Engling, G., Lee, J. J., Tsai, Y.-W., Lung, S.-C. C., Chou, C. C.-K. and Chan, C.-Y.: Size-Resolved Anhydrosugar Composition
794 in Smoke Aerosol from Controlled Field Burning of Rice Straw, *Aerosol Sci. Technol.*, 43(7), 662–672,
795 <https://doi.org/10.1080/02786820902825113>, 2009.

796 FAO: FAOSTAT, <http://www.fao.org/faostat/en/#data/QC>, last access: 21 July 2021a, 2020.

797 FAO: FAOSTAT, <http://www.fao.org/faostat/en/#data/QC>, 2020b.

798 Fomba, K. ., Müller, K., Van Pinxteren, D. and Herrmann, H.: Aerosol size-resolved trace metal composition in remote
799 northern tropical Atlantic marine environment: case study Cape Verde islands, *Atmos. Chem. Phys.*, 13(9), 4801–4814,
800 <https://doi.org/10.5194/acp-13-4801-2013>, 2013.

801 Fomba, K. W., van Pinxteren, D., Müller, K., Spindler, G. and Herrmann, H.: Assessment of trace metal levels in size-resolved
802 particulate matter in the area of Leipzig, *Atmos. Environ.*, 176, <https://doi.org/10.1016/j.atmosenv.2017.12.024>, 2018.

803 Franzin, B. T., Guizzellini, F. C., de Babos, D. V., Hojo, O., Pastre, I. A., Marchi, M. R. R., Fertoni, F. L. and Oliveira, C.
804 M. R. R.: Characterization of atmospheric aerosol (PM₁₀ and PM_{2.5}) from a medium sized city in São Paulo state, Brazil, *J.*
805 *Environ. Sci. (China)*, 89, 238–251, <https://doi.org/10.1016/j.jes.2019.09.014>, 2020.

806 Friese, E. and Ebel, A.: Temperature Dependent Thermodynamic Model of the System H + - NH₄ + - Na + - SO₄²⁻ - NO₃
807 - - Cl - - H₂O., 2010.

808 Gonçalves, C., Figueiredo, B. R., Alves, C. A., Cardoso, A. A. and Vicente, A. M.: Size-segregated aerosol chemical
809 composition from an agro-industrial region of São Paulo state, Brazil, *Air Qual. Atmos. Heal.* 2016 104, 10(4), 483–496,
810 <https://doi.org/10.1007/S11869-016-0441-0>, 2016.

811 Gondwe, M.: Comparison of modeled versus measured MSA : nss SO₄ = 4 ratios : A global analysis, , 18, 1–18,
812 <https://doi.org/10.1029/2003GB002144>, 2004.

813 H M Malcolm and Dobson, S.: The calculation of an Environmental Assessment Level (EAL) for atmospheric PAHs using
814 relative potencies., 1994.

815 Hall, D., Wu, C. Y., Hsu, Y. M., Stormer, J., Engling, G., Capeto, K., Wang, J., Brown, S., Li, H. W. and Yu, K. M.: PAHs,
816 carbonyls, VOCs and PM_{2.5} emission factors for pre-harvest burning of Florida sugarcane, *Atmos. Environ.*, 55, 164–172,
817 <https://doi.org/10.1016/j.atmosenv.2012.03.034>, 2012.

818 Hernández, J. D. R. and Mesa, Ó. J.: A simple conceptual model for the heat induced circulation over Northern South America
819 and MESO-America, *Atmosphere (Basel)*, 11(11), 1–14, <https://doi.org/10.3390/atmos1111235>, 2020.

820 Ianniello, A., Spataro, F., Esposito, G., Allegrini, I., Hu, M. and Zhu, T.: and Physics Chemical characteristics of inorganic
821 ammonium salts in PM_{2.5} in the atmosphere of Beijing (China), , (October), <https://doi.org/10.5194/acp-11-10803-2011>,
822 2011.

823 Iinuma, Y., Engling, G., Puxbaum, H. and Herrmann, H.: A highly resolved anion-exchange chromatographic method for
824 determination of saccharidic tracers for biomass combustion and primary bio-particles in atmospheric aerosol, *Atmos.*

825 Environ., 43(6), 1367–1371, 2009.

826 Jorquera, H. and Barraza, F.: Source apportionment of ambient PM_{2.5} in Santiago, Chile: 1999 and 2004 results, *Sci. Total*
827 *Environ.*, 435–436, 418–429, <https://doi.org/10.1016/j.scitotenv.2012.07.049>, 2012.

828 Jorquera, H. and Barraza, F.: Source apportionment of PM₁₀ and PM_{2.5} in a desert region in northern Chile, *Sci. Total*
829 *Environ.*, 444, 327–335, <https://doi.org/10.1016/j.scitotenv.2012.12.007>, 2013.

830 Kang, M., Ren, L., Ren, H., Zhao, Y., Kawamura, K., Zhang, H., Wei, L., Sun, Y., Wang, Z. and Fu, P.: Primary biogenic and
831 anthropogenic sources of organic aerosols in Beijing, China: Insights from saccharides and n-alkanes, *Environ. Pollut.*, 243,
832 1579–1587, <https://doi.org/10.1016/j.envpol.2018.09.118>, 2018.

833 Karagulian, F., Belis, C. A., Francisco, C., Dora, C., Prüss-üstün, A. M., Bonjour, S., Adair-rohani, H. and Amann, M.:
834 Contributions to cities ' ambient particulate matter (PM): A systematic review of local source contributions at global level,
835 *Atmos. Environ.*, 120, 475–483, <https://doi.org/10.1016/j.atmosenv.2015.08.087>, 2015.

836 Khedidji, S., Müller, K., Rabhi, L., Spindler, G., Fomba, K. W., Pinxteren, D. van, Yassaa, N. and Herrmann, H.: Chemical
837 Characterization of Marine Aerosols in a South Mediterranean Coastal Area Located in Bou Ismail, Algeria, *Aerosol Air Qual.*
838 *Res.*, 20(January), <https://doi.org/10.4209/aaqr.2019.09.0458>, 2020.

839 Kundu, S. and Stone, E. A.: Composition and sources of fine particulate matter across urban and rural sites in the Midwestern
840 United States, *Environ. Sci. Process. Impacts*, 16(6), 1360–1370, <https://doi.org/10.1039/c3em00719g>, 2014.

841 Lara, L. L., Artaxo, P., Martinelli, L. A., Camargo, P. B., Victoria, R. L. and Ferraz, E. S. B.: Properties of aerosols from
842 sugar-cane burning emissions in Southeastern Brazil, *Atmos. Environ.*, 39(26), 4627–4637,
843 <https://doi.org/10.1016/j.atmosenv.2005.04.026>, 2005.

844 Lee, S., Wang, Y. and Russell, A. G.: Assessment of secondary organic carbon in the southeastern United States: A review, *J.*
845 *Air Waste Manag. Assoc.*, 60(11), 1282–1292, <https://doi.org/10.3155/1047-3289.60.11.1282>, 2010.

846 Lee, T., Yu, X., Kreidenweis, S. M., Malm, W. C. and Collett, J. L.: Semi-continuous measurement of PM_{2.5} ionic
847 composition at several rural locations in the United States, , 42, 6655–6669, <https://doi.org/10.1016/j.atmosenv.2008.04.023>,
848 2008.

849 Li, J., Song, Y., Mao, Y., Mao, Z., Wu, Y., Li, M., Huang, X., He, Q. and Hu, M.: Chemical characteristics and source
850 apportionment of PM_{2.5} during the harvest season in eastern China's agricultural regions, *Atmos. Environ.*, 92, 442–448,
851 <https://doi.org/10.1016/J.ATMOSENV.2014.04.058>, 2014.

852 Li, X., Wang, L., Ji, D., Wen, T., Pan, Y., Sun, Y. and Wang, Y.: Characterization of the size-segregated water-soluble
853 inorganic ions in the Jing-Jin-Ji urban agglomeration: Spatial/temporal variability, size distribution and sources, *Atmos.*
854 *Environ.*, 77, 250–259, <https://doi.org/10.1016/j.atmosenv.2013.03.042>, 2013.

855 Liang, C. S., Duan, F. K., He, K. Bin and Ma, Y. L.: Review on recent progress in observations, source identifications and
856 countermeasures of PM_{2.5}, *Environ. Int.*, 86, 150–170, <https://doi.org/10.1016/j.envint.2015.10.016>, 2016.

857 Lin, L., Lee, M. L. and Eatough, D. J.: Review of recent advances in detection of organic markers in fine particulate matter
858 and their use for source apportionment, *J. Air Waste Manag. Assoc.*, 60(1), 3–25, <https://doi.org/10.3155/1047-3289.60.1.3>,

859 2010.

860 López Larada, J.: |Zona portuaria de Buenaventura: y su importancia en Colombia, Univ. San Buenaventura, 1–14
861 http://bibliotecadigital.usbcali.edu.co/bitstream/10819/7099/1/Zona_Portuaria_Buenaventura_Lopez_2017.pdf, last access:
862 23 February 2022, 2017.

863 Lopez, M. and Howell, W.: Katabatic Winds in the equatorial Andes, *J. Atmos. Sci.*, 24(1), 29–35, 1967.

864 Lyu, R., Shi, Z., Alam, M. S., Wu, X., Liu, D., Vu, T. V., Stark, C., Xu, R., Fu, P., Feng, Y. and Harrison, R. M.: Alkanes and
865 aliphatic carbonyl compounds in wintertime PM_{2.5} in Beijing, China, *Atmos. Environ.*, 202(November 2018), 244–255,
866 <https://doi.org/10.1016/j.atmosenv.2019.01.023>, 2019.

867 MADS: Res. No 2254, Ministerio de Ambiente y Desarrollo Sostenible, Colombia., 2017.

868 Majra, J. P.: Air Quality in Rural Areas, in *Chemistry, Emission Control, Radioactive Pollution and Indoor Air Quality*,
869 <https://doi.org/10.5772/16890>, , 2011.

870 Mancilla, Y., Mendoza, A., Fraser, M. P. and Herckes, P.: Organic composition and source apportionment of fine aerosol at
871 Monterrey, Mexico, based on organic markers, *Atmos. Chem. Phys.*, 16(2), 953–970, [https://doi.org/10.5194/acp-16-953-](https://doi.org/10.5194/acp-16-953-2016)
872 2016, 2016.

873 Marzi, R., Torkelson, B. E. and Olson, R. K.: A revised carbon preference index, *Org. Geochem.*, 20(8), 1303–1306,
874 [https://doi.org/10.1016/0146-6380\(93\)90016-5](https://doi.org/10.1016/0146-6380(93)90016-5), 1993.

875 Meinardi, S., Simpson, I. J., Blake, N. J., Blake, D. R. and Rowland, F. S.: Dimethyl disulfide (DMDS) and dimethyl sulfide
876 (DMS) emissions from biomass burning in Australia, *Geophys. Res. Lett.*, 30(9), <https://doi.org/10.1029/2003GL016967>,
877 2003.

878 Mesa S., Ó. J. and Rojo H., J. D.: On the general circulation of the atmosphere around Colombia, *Rev. la Acad. Colomb.*
879 *Ciencias Exactas, Fis. y Nat.*, 44(172), 857–875, <https://doi.org/10.18257/RACCEFYN.899>, 2020.

880 Miguel, A. H. and Pereira, P. A. P.: Benzo(k)fluoranthene, benzo(ghi)perylene, and indeno(1, 2, 3-cd)pyrene: New tracers of
881 automotive emissions in receptor modeling, *Aerosol Sci. Technol.*, 10(2), 292–295,
882 <https://doi.org/10.1080/02786828908959265>, 1989.

883 Min.Agricultura: Cadenas cárnicas bovina - bufalina, Bogotá D.C.
884 [https://sioc.minagricultura.gov.co/Bovina/Documentos/2018-12-30 Cifras Sectoriales.pdf](https://sioc.minagricultura.gov.co/Bovina/Documentos/2018-12-30%20Cifras%20Sectoriales.pdf), 2018.

885 Min.Agricultura: Cadena Carnica Porcina, Bogotá D.C. [https://sioc.minagricultura.gov.co/Porcina/Documentos/2019-12-30](https://sioc.minagricultura.gov.co/Porcina/Documentos/2019-12-30%20Cifras%20Sectoriales.pdf)
886 [Cifras sectoriales.pdf](https://sioc.minagricultura.gov.co/Porcina/Documentos/2019-12-30%20Cifras%20Sectoriales.pdf), 2019.

887 Min.Agricultura: Cadena Avícola, segundo trimestre 2020, Bogotá D.C.
888 <https://www.minagricultura.gov.co/paginas/default.aspx>, 2020.

889 Mugica-Alvarez, V., Santiago-de la Rosa, N., Figueroa-Lara, J., Flores-Rodríguez, J., Torres-Rodríguez, M. and Magaña-
890 Reyes, M.: Emissions of PAHs derived from sugarcane burning and processing in Chiapas and Morelos México, *Sci. Total*
891 *Environ.*, 527–528, 474–482, <https://doi.org/10.1016/j.scitotenv.2015.04.089>, 2015.

892 Mugica-Álvarez, V., Ramos-Guizar, S., Rosa, N. S. la, Torres-Rodríguez, M. and Noreña-Franco, L.: Black Carbon and

893 Particulate Organic Toxics Emitted by Sugarcane Burning in Veracruz, México, *Int. J. Environ. Sci. Dev.*, 7(4), 290–294,
894 <https://doi.org/10.7763/ijesd.2016.v7.786>, 2016.

895 Mugica-Álvarez, V., Hernández-Rosas, F., Magaña-Reyes, M., Herrera-Murillo, J., Santiago-De La Rosa, N., Gutiérrez-
896 Arzaluz, M., de Jesús Figueroa-Lara, J. and González-Cardoso, G.: Sugarcane burning emissions: Characterization and
897 emission factors, *Atmos. Environ.*, 193, 262–272, <https://doi.org/10.1016/j.atmosenv.2018.09.013>, 2018.

898 Murillo, J. H., Roman, S. R., Felix, J., Marin, R., Ramos, A. C., Jimenez, S. B., Gonzalez, B. C. and Baumgardner, D. G.:
899 Chemical characterization and source apportionment of PM₁₀ and PM_{2.5} in the metropolitan area of Costa Rica, Central
900 America Jorge, *Atmos. Pollut. Res.*, 4(2), 181–190, <https://doi.org/10.5094/APR.2013.018>, 2013.

901 Neusüss, C., Pelzing, M., Plewka, A. and Herrmann, H.: A new analytical approach for size-resolved speciation of organic
902 compounds in atmospheric aerosol particles: Methods and first results, *J. Geophys. Res. Atmos.*, 105(D4), 4513–4527,
903 <https://doi.org/10.1029/1999JD901038>, 2000.

904 Nisbet, I. C. T. and LaGoy, P. K.: Toxic equivalency factors (TEFs) for polycyclic aromatic hydrocarbons (PAHs), *Regul.*
905 *Toxicol. Pharmacol.*, 16(3), 290–300, [https://doi.org/10.1016/0273-2300\(92\)90009-X](https://doi.org/10.1016/0273-2300(92)90009-X), 1992.

906 Oros, D. R., Abas, M. R. bin, Omar, N. Y. M. J., Rahman, N. A. and Simoneit, B. R. T.: Identification and emission factors of
907 molecular tracers in organic aerosols from biomass burning: Part 3. Grasses, *Appl. Geochemistry*, 21(6), 919–940,
908 <https://doi.org/10.1016/j.apgeochem.2006.01.008>, 2006.

909 Orozco, C., Sanandres, E. and Molinares, I.: Colombia, Panamá y la Ruta Panamericana: Encuentros y Desencuentros,
910 *Memorias Rev. Digit. Hist. y Arqueol. desde el Caribe*, 16(ISSN 1794-8886)
911 http://www.scielo.org.co/scielo.php?script=sci_arttext&pid=S1794-88862012000100005, last access: 23 February 2022,
912 2012.

913 Ortiz, E. Y., Jimenez, R., Fochesatto, G. J. and Morales-Rincon, L. A.: Caracterización de la turbulencia atmosférica en una
914 gran zona verde de una megaciudad andina tropical, *Rev. la Acad. Colomb. Ciencias Exactas, Físicas y Nat.*, 43(166), 133,
915 <https://doi.org/10.18257/raccefyn.697>, 2019.

916 Pant, P. and Harrison, R. M.: Estimation of the contribution of road traffic emissions to particulate matter concentrations from
917 field measurements: A review, *Atmos. Environ.*, 77, 78–97, <https://doi.org/10.1016/j.atmosenv.2013.04.028>, 2013.

918 Pereira, G. M., Teinilä, K., Custódio, D., Gomes Santos, A., Xian, H., Hillamo, R., Alves, C. A., Bittencourt de Andrade, J.,
919 Olímpio da Rocha, G., Kumar, P., Balasubramanian, R., Andrade, M. de F. and de Castro Vasconcellos, P.: Particulate
920 pollutants in the Brazilian city of São Paulo: 1-year investigation for the chemical composition and source apportionment,
921 *Atmos. Chem. Phys.*, 17(19), 11943–11969, <https://doi.org/10.5194/acp-17-11943-2017>, 2017.

922 Pereira, G. M., Oraggio, B., Teinilä, K., Custódio, D., Huang, X., Hillamo, R., Alves, C. A., Balasubramanian, R., Rojas, N.
923 Y. and Sanchez-Ccoyllo, O.: A comparative chemical study of PM₁₀ in three Latin American cities : Lima, Medellín, ans São
924 Paulo, *Air Qual. Atmos. Heal.*, 12, 1141–1152, <https://doi.org/10.1007/s11869-019-00735-3>, 2019.

925 Pio, C., Cerqueira, M., Harrison, R. M., Nunes, T., Mirante, F., Alves, C., Oliveira, C., Sanchez de la Campa, A., Artífiano, B.
926 and Matos, M.: OC/EC ratio observations in Europe: Re-thinking the approach for apportionment between primary and

927 secondary organic carbon, *Atmos. Environ.*, 45(34), 6121–6132, <https://doi.org/10.1016/j.atmosenv.2011.08.045>, 2011.

928 Plaza, J., Artñano, B., Salvador, P., Gómez-Moreno, F. J., Pujadas, M. and Pio, C. A.: Short-term secondary organic carbon
929 estimations with a modified OC/EC primary ratio method at a suburban site in Madrid (Spain), *Atmos. Environ.*, 45(15), 2496–
930 2506, <https://doi.org/10.1016/j.atmosenv.2011.02.037>, 2011.

931 Pye, H. O. T., Nenes, A., Alexander, B., Ault, A. P., Barth, M. C., Clegg, S. L., Collett, J. L., Fahey, K. M., Hennigan, C. J.,
932 Herrmann, H., Kanakidou, M., Kelly, J. T., Ku, I. T., Faye McNeill, V., Riemer, N., Schaefer, T., Shi, G., Tilgner, A., Walker,
933 J. T., Wang, T., Weber, R., Xing, J., Zaveri, R. A. and Zuend, A.: The acidity of atmospheric particles and clouds., 2020.

934 Ramírez, O., Sánchez de la Campa, A. M., Amato, F., Catacolí, R. A., Rojas, N. Y. and de la Rosa, J.: Chemical composition
935 and source apportionment of PM10 at an urban background site in a high–altitude Latin American megacity (Bogota,
936 Colombia), *Environ. Pollut.*, 233, 142–155, <https://doi.org/10.1016/j.envpol.2017.10.045>, 2018.

937 Ravindra, K., Sokhi, R. and Van Grieken, R.: Atmospheric polycyclic aromatic hydrocarbons: Source attribution, emission
938 factors and regulation, *Atmos. Environ.*, 42(13), 2895–2921, <https://doi.org/10.1016/j.atmosenv.2007.12.010>, 2008.

939 Romero, D., Sarmiento, H. and Pachón, J. E.: Estimación de hidrocarburos aromáticos policíclicos y metales pesados asociados
940 con la quema de caña de azúcar en el valle geográfico del río Cauca , Colombia, *Rev. Épsilon*, 21(2013), 57–82, 2013.

941 RUNT. (2021). [Vehicles fleet dataset Cauca Valley Department] [Unpublished raw data]. Registro Unico del Transito.

942 Ryu, S. Y., Kim, J. E., Zhuanshi, H., Kim, Y. J. and Kang, G. U.: Chemical composition of post-harvest biomass burning
943 aerosols in gwangju, Korea, *J. Air Waste Manag. Assoc.*, 54(9), 1124–1137,
944 <https://doi.org/10.1080/10473289.2004.10471018>, 2004.

945 Dos Santos, C. Y. M., Azevedo, D. de A. and De Aquino Neto, F. R.: Selected organic compounds from biomass burning
946 found in the atmospheric particulate matter over sugarcane plantation areas, *Atmos. Environ.*, 36(18), 3009–3019,
947 [https://doi.org/10.1016/S1352-2310\(02\)00249-2](https://doi.org/10.1016/S1352-2310(02)00249-2), 2002.

948 Schauer, J. J.: Sources contributions to atmospheric organic compound concentrations: Emissions measurments and model
949 predictions, California Institute Technology, 1998.

950 SDA: Plan decenal de descontaminación del aire de Bogotá, Bogotá D.C.
951 [http://ambientebogota.gov.co/en/c/document_library/get_file?uuid=b5f3e23f-9c5f-40ef-912a-](http://ambientebogota.gov.co/en/c/document_library/get_file?uuid=b5f3e23f-9c5f-40ef-912a-51a5822da320&groupId=55886)
952 [51a5822da320&groupId=55886](http://ambientebogota.gov.co/en/c/document_library/get_file?uuid=b5f3e23f-9c5f-40ef-912a-51a5822da320&groupId=55886), 2010.

953 Seinfeld, J. H. and Pandis, S. N.: *Atmospheric From Air Pollution to Climate Change.*, 2006.

954 SICOM: Boletín estadístico, Boletín Estad. EDS automotriz y Fluv. <https://www.sicom.gov.co/index.php/boletin-estadistico>,
955 last access: 15 February 2022, 2018.

956 Simoneit, B. R. T.: Biomass burning - A review of organic tracers for smoke from incomplete combustion, *Appl.*
957 *Geochemistry*, 17(3), 129–162, [https://doi.org/10.1016/S0883-2927\(01\)00061-0](https://doi.org/10.1016/S0883-2927(01)00061-0), 2002.

958 Snider, G., Weagle, C. L., Murdymootoo, K. K., Ring, A., Ritchie, Y., Stone, E., Walsh, A., Akoshile, C., Anh, N. X.,
959 Balasubramanian, R., Brook, J., Qonitan, F. D., Dong, J., Griffith, D., He, K., Holben, B. N., Kahn, R., Lagrosas, N., Lestari,
960 P., Ma, Z., Misra, A., Norford, L. K., Quel, E. J., Salam, A., Schichtel, B., Segev, L., Tripathi, S., Wang, C., Yu, C., Zhang,

961 Q., Zhang, Y., Brauer, M., Cohen, A., Gibson, M. D., Liu, Y., Martins, J. V., Rudich, Y. and Martin, R. V.: Variation in global
962 chemical composition of PM_{2.5}: emerging results from SPARTAN, *Atmos. Chem. Phys.*, 16(15), 9629–9653,
963 <https://doi.org/10.5194/acp-16-9629-2016>, 2016.

964 Sorooshian, A., Crosbie, E., Maudlin, L. C., Youn, J., Wang, Z., Shingler, T., Ortega, A. M., Hersey, S. and Woods, R. K.:
965 Surface and airborne measurements of organosulfur and methanesulfonate over the western United States and coastal areas, *J.*
966 *Geophys. Res. Atmos.*, 8535–8548, <https://doi.org/10.1002/2015JD023822>.Received, 2015.

967 Souza, D. Z., Vasconcellos, P. C., Lee, H., Aurela, M., Saarnio, K., Teinilä, K. and Hillamo, R.: Composition of PM_{2.5} and
968 PM₁₀ collected at Urban Sites in Brazil, *Aerosol Air Qual. Res.*, 14(1), 168–176, <https://doi.org/10.4209/aaqr.2013.03.0071>,
969 2014.

970 Stahl, C., Cruz, M. T., Bañaga, P. A., Betito, G., Braun, R. A., Aghdam, M. A., Cambaliza, M. O., Lorenzo, G. R., Macdonald,
971 A. B., Hilario, M. R. A., Pabroa, P. C., Yee, J. R. and Simpas, J. B.: Sources and characteristics of size-resolved particulate
972 organic acids and methanesulfonate in a coastal megacity : Manila , Philippines, , 15907–15935, 2020.

973 Sutton, M. A., Billen, G., Bleeker, A., Erisman, J. W., Grennfelt, P., Grinsven, H. Van, Grizzetti, B., Howard, C. M. and Leip,
974 A.: Technical summary Part I Nitrogen in Europe : the present position, *Eur. Nitrogen Assess. Sources, Eff. Policy Perspect.*,
975 (December 2015), Xxxv–Lii, <https://doi.org/10.1017/CBO9780511976988.003>, 2011.

976 Szabó, J., Szabó Nagy, A. and Erdős, J.: Ambient concentrations of PM₁₀, PM₁₀-bound polycyclic aromatic hydrocarbons
977 and heavy metals in an urban site of Győr, Hungary, *Air Qual. Atmos. Heal.*, 8(2), 229–241, [https://doi.org/10.1007/s11869-](https://doi.org/10.1007/s11869-015-0318-7)
978 015-0318-7, 2015.

979 Tang, M., Guo, L., Bai, Y., Huang, R., Wu, Z. and Wang, Z.: Impacts of methanesulfonate on the cloud condensation
980 nucleation activity of sea salt aerosol, *Atmos. Environ.*, 201(October 2018), 13–17,
981 <https://doi.org/10.1016/j.atmosenv.2018.12.034>, 2019.

982 Tobiszewski, M. and Namieśnik, J.: PAH diagnostic ratios for the identification of pollution emission sources, *Environ. Pollut.*,
983 162(November 2018), 110–119, <https://doi.org/10.1016/j.envpol.2011.10.025>, 2012.

984 Tsigaridis, K., Daskalakis, N., Kanakidou, M., Adams, P. J., Artaxo, P., Bahadur, R., Balkanski, Y., Bauer, S. E., Bellouin,
985 N., Benedetti, A., Bergman, T., Berntsen, T. K., Beukes, J. P., Bian, H., Carslaw, K. S., Chin, M., Curci, G., Diehl, T., Easter,
986 R. C., Ghan, S. J., Gong, S. L., Hodzic, A., Hoyle, C. R., Iversen, T., Jathar, S., Jimenez, J. L., Kaiser, J. W., Kirkevåg, A.,
987 Koch, D., Kokkola, H., H Lee, Y., Lin, G., Liu, X., Luo, G., Ma, X., Mann, G. W., Mihalopoulos, N., Morcrette, J. J., Müller,
988 J. F., Myhre, G., Myriokefalitakis, S., Ng, N. L., O'donnell, D., Penner, J. E., Pozzoli, L., Pringle, K. J., Russell, L. M., Schulz,
989 M., Sciare, J., Seland, Shindell, D. T., Sillman, S., Skeie, R. B., Spracklen, D., Stavrou, T., Steenrod, S. D., Takemura, T.,
990 Tiitta, P., Tilmes, S., Tost, H., Van Noije, T., Van Zyl, P. G., Von Salzen, K., Yu, F., Wang, Z., Wang, Z., Zaveri, R. A.,
991 Zhang, H., Zhang, K., Zhang, Q. and Zhang, X.: The AeroCom evaluation and intercomparison of organic aerosol in global
992 models, *Atmos. Chem. Phys.*, 14(19), 10845–10895, <https://doi.org/10.5194/acp-14-10845-2014>, 2014.

993 Turpin, B. J. and Lim, H.: Species Contributions to PM_{2.5} Mass Concentrations : Revisiting Common Assumptions for
994 Estimating Organic Mass, *Aerosol Sci. Technol.*, 35:1(September 2014), 37–41,
37

995 <https://doi.org/http://dx.doi.org/10.1080/02786820119445>, 2010.

996 Urban, R. C., Alves, C. A., Allen, A. G., Cardoso, A. A., Queiroz, M. E. C. and Campos, M. L. A. M.: Sugar markers in aerosol
997 particles from an agro-industrial region in Brazil, *Atmos. Environ.*, 90(2014), 106–112,
998 <https://doi.org/10.1016/j.atmosenv.2014.03.034>, 2014.

999 Urban, R. C., Alves, C. A., Allen, A. G., Cardoso, A. A. and Campos, M. L. A. M.: Organic aerosols in a Brazilian agro-
1000 industrial area: Speciation and impact of biomass burning, *Atmos. Res.*, 169, 271–279,
1001 <https://doi.org/10.1016/j.atmosres.2015.10.008>, 2016.

1002 Vargas, F. A., Rojas, N. Y., Pachon, J. E. and Russell, A. G.: PM10 characterization and source apportionment at two
1003 residential areas in Bogota, *Atmos. Pollut. Res.*, 3(1), 72–80, <https://doi.org/10.5094/APR.2012.006>, 2012.

1004 Vasconcellos, P. C., Balasubramanian, R., Bruns, R. E., Sanchez-Ccoyllo, O., Andrade, M. F. and Flues, M.: Water-soluble
1005 ions and trace metals in airborne particles over urban areas of the state of São Paulo, Brazil: Influences of local sources and
1006 long range transport, *Water. Air. Soil Pollut.*, 186(1–4), 63–73, <https://doi.org/10.1007/s11270-007-9465-2>, 2007.

1007 Vasconcellos, P. C., Souza, D. Z., Ávila, S. G., Araújo, M. P., Naoto, E., Nascimento, K. H., Cavalcante, F. S., Dos, M.,
1008 Smichowski, P. and Behrentz, E.: Comparative study of the atmospheric chemical composition of three South American cities,
1009 *Atmos. Environ.*, 45(32), 5770–5777, <https://doi.org/10.1016/j.atmosenv.2011.07.018>, 2011.

1010 Victoria, J., Amaya, A., Rangel, H., Viveros, C., Cassalet, C., Carbonell, J., Quintero, R., Cruz, R., Isaacs, C., Larrahondo, J.,
1011 Moreno, C., Palma, A., Posada, C., Villegas, F. and Gómez, L.: Características agronómicas y de productividad de la variedad
1012 Cenicaña Colombiana (CC) 85-92, Cali., 2002.

1013 Villalobos, A. M., Barraza, F., Jorquera, H. and Schauer, J. J.: Chemical speciation and source apportionment of fine particulate
1014 matter in Santiago, Chile, 2013, *Sci. Total Environ.*, 512–513, 133–142, <https://doi.org/10.1016/j.scitotenv.2015.01.006>, 2015.

1015 Wadinga Fomba, K., Deabji, N., El Islam Barcha, S., Ouchen, I., Mehdi Elbaramoussi, E., Cherkaoui El Moursli, R., Harnafi,
1016 M., El Hajjaji, S., Mellouki, A. and Herrmann, H.: Application of TXRF in monitoring trace metals in particulate matter and
1017 cloud water, *Atmos. Meas. Tech.*, 13(9), 4773–4790, <https://doi.org/10.5194/amt-13-4773-2020>, 2020.

1018 Wagner, R., Jähn, M. and Schepanski, K.: Wildfires as a source of airborne mineral dust - Revisiting a conceptual model using
1019 large-eddy simulation (LES), *Atmos. Chem. Phys.*, 18(16), 11863–11884, <https://doi.org/10.5194/acp-18-11863-2018>, 2018.

1020 Wang, Y., Yang, F., Li, X., Tian, M. and Hopke, P. K.: On the source contribution to Beijing PM2.5 concentrations, , 134, 84–
1021 95, <https://doi.org/10.1016/j.atmosenv.2016.03.047>, 2016.

1022 WHO Regional Office for Europe: Air quality guidelines for Europe, pp. 457–465, World Health Organization, Copenhagen,
1023 Denmark, <https://doi.org/10.1525/9780520948068-070>, , 2020.

1024 World Health Organization: Review of evidence on health aspects of air pollution - REVIHAAP Project.
1025 [http://www.euro.who.int/pubrequest%0Ahttp://www.euro.who.int/__data/assets/pdf_file/0004/193108/REVIHAAP-Final-](http://www.euro.who.int/pubrequest%0Ahttp://www.euro.who.int/__data/assets/pdf_file/0004/193108/REVIHAAP-Final-technical-report-final-version.pdf)
1026 [technical-report-final-version.pdf](http://www.euro.who.int/pubrequest%0Ahttp://www.euro.who.int/__data/assets/pdf_file/0004/193108/REVIHAAP-Final-technical-report-final-version.pdf), 2013.

1027 World Health Organization: WHO global air quality guidelines: particulate matter (PM2.5 and PM10), ozone, nitrogen dioxide,
1028 sulfur dioxide and carbon monoxide, World Health Organization. <https://www.who.int/publications/i/item/9789240034228>,

1029 last access: 22 February 2022, 2021.

1030 Wu, C. and Zhen Yu, J.: Evaluation of linear regression techniques for atmospheric applications: The importance of appropriate
1031 weighting, *Atmos. Meas. Tech.*, 11(2), 1233–1250, <https://doi.org/10.5194/amt-11-1233-2018>, 2018.

1032 Xue, J., Lau, A. K. H. and Yu, J. Z.: A study of acidity on PM_{2.5} in Hong Kong using online ionic chemical composition
1033 measurements, *Atmos. Environ.*, 45(39), 7081–7088, <https://doi.org/10.1016/j.atmosenv.2011.09.040>, 2011.

1034 Yadav, I. C. and Devi, N. L.: Biomass burning, regional air quality, and climate change, *Encycl. Environ. Heal.*, (April), 386–
1035 391, <https://doi.org/10.1016/B978-0-12-409548-9.11022-X>, 2019.

1036 Yadav, S., Tandon, A. and Attri, A. K.: Monthly and seasonal variations in aerosol associated n-alkane profiles in relation to
1037 meteorological parameters in New Delhi, India, *Aerosol Air Qual. Res.*, 13(1), 287–300,
1038 <https://doi.org/10.4209/aaqr.2012.01.0004>, 2013.

1039 Yan, J., Wang, L., Fu, P. P. and Yu, H.: Photomutagenicity of 16 polycyclic aromatic hydrocarbons from the US EPA priority
1040 pollutant list, *Mutat. Res. - Genet. Toxicol. Environ. Mutagen.*, 557(1), 99–108,
1041 <https://doi.org/10.1016/j.mrgentox.2003.10.004>, 2004.

1042 Yunker, M. B., Macdonald, R. W., Vingarzan, R., Mitchell, H., Goyette, D. and Sylvestre, S.: PAHs in the Fraser River basin:
1043 a critical appraisal of PAH ratios as indicators of PAH source and composition, *Org. Geochem.*, 33, 489–515,
1044 [https://doi.org/doi.org/10.1016/S0146-6380\(02\)00002-5](https://doi.org/doi.org/10.1016/S0146-6380(02)00002-5), 2002.

1045